# Molecular Dynamics Study of Nano-confinement Effect on Hydrocarbons Fluid Phase Behavior and Composition in Organic Shale

Deraldo de Carvalho Jacobina Andrade

Thesis submitted to the faculty of the Virginia Polytechnic Institute and State University in partial fulfillment of the requirements for the degree of

Master of Science

In

Mining Engineering

Dr. Bahareh Nojabaei, Chair

Nino Ripepi

Cheng Chen

January 14, 2021

Blacksburg, Virginia

Keywords: Molecular Dynamics Simulation, unconventional reservoir, shale, hydrocarbon, phase behavior, composition, density, oil in place, nanopore

# Molecular Dynamics Study of Nano-confinement Effect on Hydrocarbons Fluid Phase Behavior and Composition in Organic Shale

Deraldo de Carvalho Jacobina Andrade

## ABSTRACT

The depletion of conventional oil reservoirs forced companies and consequently researchers to pursue alternatives such as resources that in the past were considered not economically viable, in consequence of the high depth, low porosity and permeability of the play zone. The exploration challenges were overcome mainly by the development of horizontal drilling and hydraulic fracturing. However, the extremely high temperatures and pressures, in association to a complex nanopore structure, in which reservoir fluids are now encountered, instigate further investigation of fluid phase behavior and composition, and challenge conventional macroscale reservoir simulation predictions. Moreover, the unusual high temperatures and pressures have increased the cost as well as the hazardous level for reservoir analyzes by lab experiments. Molecular Dynamics (MD) simulation of reservoirs can be a safe and inexpensive alternative tool to replicate reservoir pore and fluid conditions, as well as to monitor fluid behavior.

In this study, a MD simulation of nanoconfinement effect on hydrocarbon fluid phase and compositional behavior in organic shale rocks is presented. Chapter 1 reviews and discusses previous works on MD simulations of geological resources. With the knowledge acquired, a fully atomistic squared graphite pore is proposed and applied to study hydrocarbon fluid phase and compositional behavior in organic shale rocks in Chapter 2. Results demonstrate that nano-confinement increases fluid mass density, which can contribute to phase transition, and heptane composition inside studied pores. The higher fluid density results in an alteration of oil in place (OIP) prediction by reservoir simulations, when nano-confinement effect is not considered.

Molecular Dynamics Study of Nanoconfinement Effect on Hydrocarbons Fluid Phase Behavior and Composition in Organic Shale

Deraldo de Carvalho Jacobina Andrade

## GENERAL AUDIENCE ABSTRACT

Petroleum sub products are present in the day to day life of almost any human. The list include gasoline, plastics, perfumes, medications, polyester for clothing. Petroleum is naturally encountered in the void space, known as pores, inside rocks at reservoirs thousands of feet underground. In the past, the pores of oil reservoirs in development were larger and interconnected, which facilitates its extraction and reserve predictions. Most of reservoirs being developed nowadays have pores in the nanoscale and with poor interconnection as well as higher reservoir temperatures and pressure. These “new conditions”, instigates further investigation of fluid phase behavior and composition, and challenge macroscale reservoir simulation predictions.

In this study, the effect of decrease in pore size, as well as higher temperature and pressure conditions, in fluid behavior and composition is studied. Chapter 1 reviews and discusses previous works on geological resources modeling and simulation. With the knowledge acquired, a fully squared shale pore is proposed and applied to study hydrocarbon fluid phase and compositional behavior in organic shale rocks in Chapter 2. Results demonstrate that pores in the nanoscale region tend to increase fluid mass density, which can contribute to phase transition, and heptane composition inside studied pores. The higher fluid density results in an underestimation of reserves prediction by reservoir simulations, when the change in density is not considered.

# ACKNOWLEDGMENTS

I would like to acknowledge everyone who played a role in my academic accomplishments. First of all, to my parents, family and friends for all the love given through this time. Secondly, my advisor Dr. Nojabaei and my committee members Dr. Ripepi, and Dr. Chen, for all the guidance, support and patience during this study. Thirdly, the United Stated Department (DOE) of energy for partially funding this project. Fourthly, to the Advanced Research Computing at Virginia Tech for allowing me to use their computer system to run the simulations. Finally, I would like to acknowledge the Coordenação de Aperfeiçoamento de Pessoal de Nível Superior – Brasil (CAPES/CNPq), for partially funding my undergraduate program, and for the support during my academic life.

**Table of Contents**

**List of Figures**

**List of Tables**

# 1. Review of Molecular Dynamics Simulation of Rock-Fluid Interactions in Geological Resources

## 1.1. Introduction

Simulation of rock-fluid interactions in the rock porous media of geological resources has proved to be a challenge as both fluids and rocks involved in such systems are diverse and the involved processes and mechanisms are complicated. The porous media can be composed of various minerals such as quartz, calcite, feldspar, mica, and the organic compounds. Fluids in such systems include water, hydrocarbons, $CO_2$, $N_2$ and $H_2$. Further, the network of connected channels in porous media has a complex structure and geometry. Depending on the rock and fluid type, as well as permeability and porosity of the rock, transport fluid transport in the rock matrix can be different, ranging from high velocity convective flow to very slow diffusive mass transfer. Phase behavior of fluids may also deviate from the bulk at low permeability and in nano-sized pores.

Macroscopic modeling methods cannot capture the above described complex processes and mechanism and a micro-scale investigation approach seems more suited to better understand such complex systems. Destructive high-resolution three-dimensional imaging technics, such as Focused Ion Beam Scanning Electron Microscope (FIB-SEM) do not provide a useful answer either, since they only work with dry rock samples and in vacuum conditions, and visualization of multiphase multicomponent fluids in nanopores at reservoir pressure and temperature is not possible. High-resolution X-ray computed tomography (CT) non-destructive imaging tools might be an alternative option to investigate fluid phase behavior and transport in pores, however, they have limited resolution and magnification.

Molecular scale numerical simulation is likely the most accurate and suitable method to investigate the interactions of rock (pore wall) surface, water, oil and gas in porous media. Among

molecular simulation methods, molecular dynamics simulation (MD) is a powerful tool, which can simulate the behavior of a system in molecular scale by solving the Newton's equations of motion for each individual molecule to find the new position of that molecule with respect to others. Pore structure is usually simplified in the form of slits, circular, squared, or triangular cross-sectional shapes, while in reality there is a combination of all of these shapes in the same pore. The fluid molecules structures and force field choices can drastically change the result of a simulation, and they should be acquired from experiments. Computational cost of molecular dynamics simulation is also important and there is always a tradeoff between the computational expenses and accuracy. As a result, researchers need to represent complicated systems by simplified/focused models, and at the same time, assure that the important pore-fluid interactions, thermodynamics behavior of fluids, and flow characteristics are considered in the analyses.

Here, the molecular dynamics research studies investigating rock-fluid interactions in the porous rock of geological resources are reviewed, and the methods and parameters, including choosing different force fields, ensembles, and structures that different research groups have applied are discussed. Last, the MD measurement methods to quantify the important parameters for geological resources assessment, such as fluid density, contact angle and diffusion coefficients are explained.

### 1.2. Molecular Structure and Force Fields

In this section, the porous media, pore geometry, fluid molecules, and wettability structural design for MD representation of geological resources are discussed, and the relevant force field choices are presented and analyzed.

### 1.2.1. Porous media and rock types

The rock porous media is composed of multiple minerals (quartz, calcite, feldspar, and mica) and organic matter (kerogen with diverse maturity levels). These elements have complicated structures, which are difficult to simulate precisely using MD and researchers have proposed different approaches to represent them. Leonard Jones (LJ) hard spheres are particles where the user assigns the sphere radius and interaction energy between other atoms involved in the simulation, which are usually acquired from experimental data or ab-initio simulations. For instance, a single sphere can represent four $H_2O$ molecules or a pore wall grain, and a bundle of spheres is used to represent dodecane or a surfactant molecule [12]. These spheres can also be organized in a lattice, such as face centered cubic (fcc) [24], or in a coarse grained model [12,16], as proposed by Marrink *et al*. [30,31] (**Figure 1.1**). This is a simplistic approach, and constructed pore walls by these spheres overlook some important parameters, such as: friction (they have smooth shape), individual interaction of atoms composing the walls and fluid atoms. This can lead to underestimation/overestimation of properties such as threshold capillary pressure, contact angle, fluid velocity and viscosity. On the other hand, simulations are much less computationally expensive and still different cross sections and shapes can be modeled.

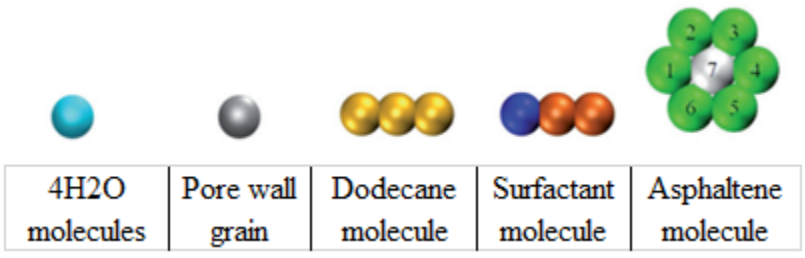


**Figure 1.1:** Coarse grained representation of LJ particles [12].

More complicated models have used the real crystal structure and lattice parameters from common minerals encountered in oil reservoirs, such as silica [3,14,18,19,26], calcite [11,20], and mica [5,10,28] (**Figure 1.2**). The crystal structure of these minerals are readily available from the online crystallography databases [32,33] on Crystallographic Information Framework (CIF) format. After choosing the mineral, researchers have to decide in what orientation they want to cleave the crystal. This directly interferes in how the fluid molecules interact (adsorb for instance) with the surface since different cleaving directions expose different atoms on the surface. For instance, to model silica, the most widely used crystal is the α-quartz ($SiO_2$) cleaved along (001) crystallographic orientation [3,6,14,19,26]. To the best of our knowledge, there is no work that has combined minerals in MD simulation, as it is hard to predict bonds, partial charges and interaction parameters for the crystals combination, even in experiments or ab-initio works. By using this type of approach, researchers can compare and validate their models to experimental data, such as the surface density of –OH [3,6] or silanol [18,26] groups. The partial charges and interaction energy for each individual atom are assigned from force fields (FF) with parameters acquired from ab-initial MD works, which are much more reliable since the electrons are taken into account. The most common force field is CLAYFF [34], which was developed for hydrated and multicomponent minerals, as well as their interface with fluids, which explain why it is widely used for mica and some silica models. For calcite, the force fields proposed by Xiao [22] *et al*., or Raiteri [12], where the most common choices. Raiteri's force field, however, was fitted to better represent the thermodynamics properties of calcite rather than its mechanical properties. As expected, this approach is much more computationally expensive, and pore geometries other than slit-pores (more on this on pore geometry section) are difficult to model accurately.

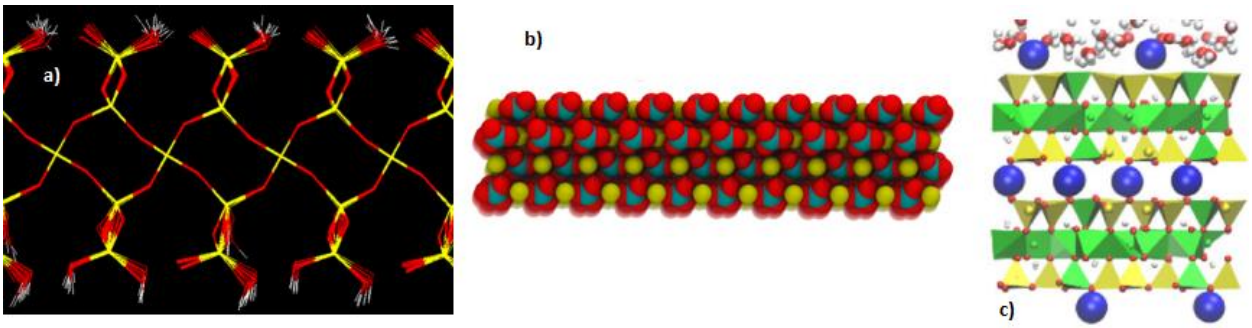


**Figure 1.2:** Models for different minerals. a) Quartz [26], b) Calcite [20], and c) Mica [10].

The organic matter of the rock has been mainly simulated in two ways. The first one is to use graphene walls, a layer of $sp^2$ bonded carbons arranged on a hexagonal lattice. Normally these models used multiple layers of graphene, sometimes called graphite, in order to make the thickness of the wall greater than the cutoff distance. Graphite is normally encountered in shale reservoirs, and its carbon-only composition makes the simulation less computationally expensive, while being a justifiable path. The second approach is the simulation of Type II kerogen [38,39] since this is the most common kerogen type that is present in oil and gas reservoirs [38]. To create a wall, eight kerogen layers are placed in a simulation box, and then compressed under reservoir pressure and temperature, and the result of the simulation is used as a slit-pore wall [39]. **Figure 1.3** (b) shows the result of this approach. The main differences of the approaches are that the second takes in consideration heteroatoms content and roughness. When heteroatoms, such as Oxygen, Nitrogen, and Sulfur, are present in the porous media, a more hydrophilic behavior is expected since O and N can make hydrogen bonds with water, while a hydrophobic behavior is encountered when only carbon atoms are present in the rock. The wettability and roughness of the solid molecules greatly influences the adsorption behavior of molecules on the pore walls [36].

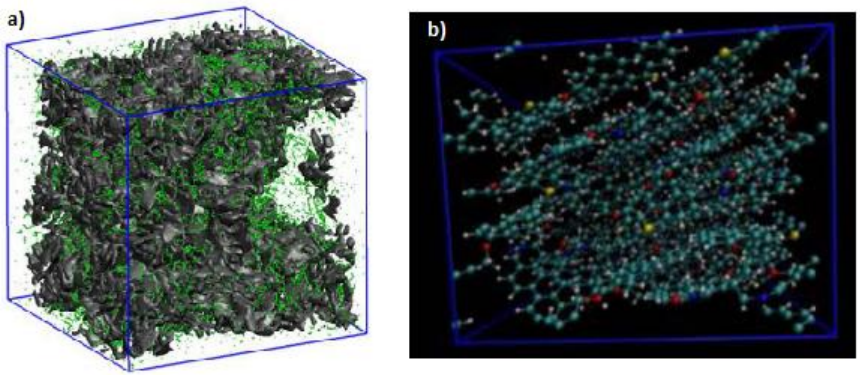


**Figure 1.3:** Kerogen models a) type II kerogen formed by oil molecules [38], b) type II kerogen formed by graphene oxide [39].

### 1.2.2. Pore geometry

The channels through which fluids flow in oil reservoirs often have tortuous paths with complicated cross sectional shapes and realistic representation of such porous media has been a challenge for researchers using MD simulation tools. However, three approaches have been somewhat successful in the area: slit-pores (more simplistic, faster), nanotubes, and the "block carving" approach (more robust, expensive).

Slit-pores consist of two parallel disconnected and independent solid slabs that are placed with void space relative to each other. Each slab acts as the wall of the pore, while the spacing is the pore space (**Figure 1.4**). The wall is infinite in the direction perpendicular to the flow because of periodic boundary conditions. This is by far the most used approach, and there are works with diverse materials: graphene [8,9], silica [3,4,6,14,15], calcite [11,20], mica [5,10,28], and kerogen [38,39]. It is relatively simple to change the distance between the slabs, which consequently makes the study on the effect of slit aperture/pore size in fluid and flow properties straightforward. In addition, since only two walls are present (compared to a surrounding wall with three or more sides), less atoms are present in the simulation box, which makes the simulation less

computationally expensive. However, the absence of walls can lead to underestimation of threshold capillary pressure, friction, and interaction between solid-fluid molecules.

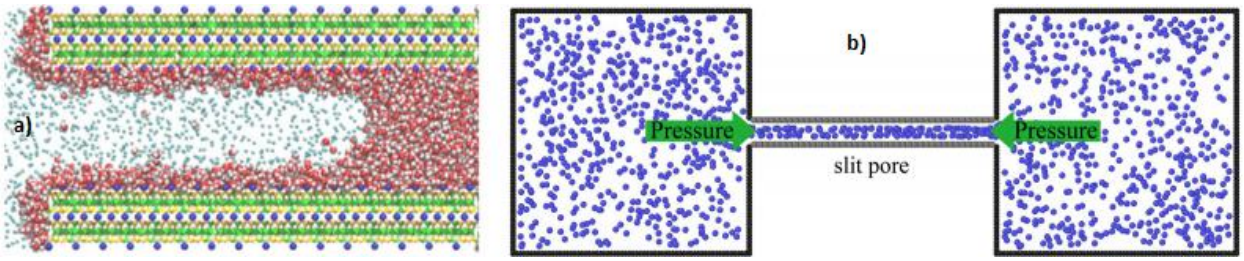


**Figure 1.4:** Slit pores in a) mica [10] and b) graphene [13].

More realistic models, in terms of presence of all walls, are represented by nanotubes and block carving approach (**Figure 1.5**). Using the nanotubes provide a smooth way to represent the pores on organic matter present in the rock matrix. It is easy to control the aperture size, and cylindrical and conical shapes [1] can be used. Software such as Nanotube Modeler [40] can readily generate concentrically organized nanotubes with different radius. The disadvantage of this method is that heteroatoms are not usually considered, and friction is underestimated. Another approach is to carve out holes from a block of LJ spheres [12], or actual crystal supercell3 [3,6,16]. For the first, only removing the atoms from a predefined radius from the center of the pore is necessary, but for the latter carving approach, it is necessary to add (-OH) or (-H) radicals to the dangling bonds. This is justified by the fact that water interacts initially with the reservoir minerals before the start of any hydrocarbon accumulation. Even though this is the closest to reality, it still encounters many problems with the predictions of partial charges, and interactions parameters for atoms on the surface, as the carved hole has numerous molecules to be studied by ab-initio MD

simulations, while it is extremely difficult to be validated by experiments, which may make it even less realistic than slit-pores.

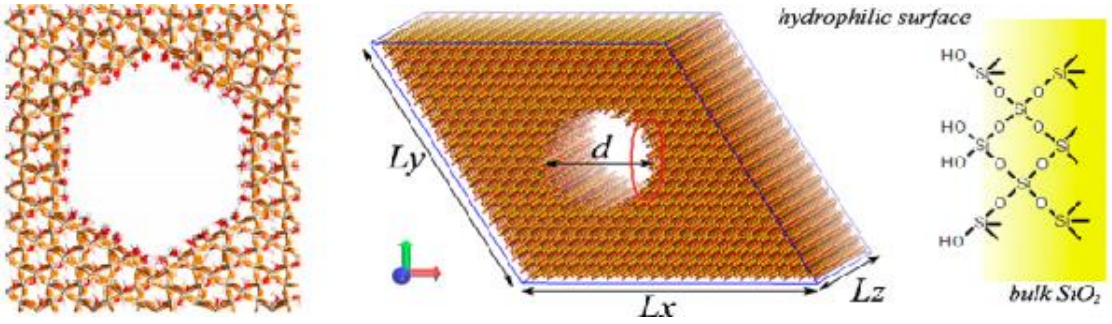


**Figure 1.5:** Circular shaped super crystal cell structures, where is a) in focus [4] and a pore view [15].

### 1.2.3. Fluid molecules

Computational cost is always a concern in MD simulations, as it was demonstrated on last sections, but for fluid molecules this factor is even more crucial since they usually are the most abundant molecules in the simulation. In general, three main ways have been used to represent fluid molecules. One approach is to use a coarse grained model, where the structure of the molecule is ignored, and the molecules are represented by beads [8,12,16] and **Figure 1** represents this case. The second approach is the united atom (UA) [14,17,20,22,24,25], where the hydrogens are treated implicitly, for example, -$CH_3$ and -$CH_2$- groups in alkanes are treated as one particle with only one potential parameter and zero charge. The third approach, all atom (AA), is where all the atoms are defined separately and receive an individual potential parameter and partial charge. Here is the discussion of the most common force fields and molecules structures used to represent the fluid molecules.

#### 1.2.3.1. Hydrocarbon Molecules

The composition of oil inside pores varies significantly from an almost pure methane to a complex heavy mixture of alkanes, naphthenes, aromatic, and asphaltic molecules. Researchers chose oil composition by either targeting a specific reservoir to analyze [19,22], or by a phenomenon they want to study [12,13]. Since there has been a rise in extraction of natural gas from shales [15], the majority of studies use methane [12,18] as the hydrocarbon molecule to be analyzed. They used mostly Optimized Potentials for Liquid Simulation (OPLS)-(UA [14,25] or AA [15,26]) FF since its parameters were acquired from matching experimental data [18] and it has a good representation for organic molecules [15]. Following the same trend, other research studies tried to reproduce shale oils. However, the majority chose to simulate only a single molecule to represent petroleum, such as n-heptane [17,22], n-octane [14], or dodecane [6,12], and their explanation was that the density of these molecules is comparable to the average shale oil densities. It is important to highlight here that this is a simplistic approach and it definitely does not represent the detailed oil composition, however, researchers were mostly interested in studying the fluid flow, which would be much more complicated and computationally expensive if a complex mixture had been used. On the other hand, papers that concentrated on adsorption/desorption or just wanted a more realistic approach have used a multicomponent mixture. For instance, a model proposed by Matsuoka et al.[15], includes hexane, heptane, octane, nonane, cyclohexane, cycloheptane, toluene and benzene. Wu et al. [7] analyzed the desorption of a kerogen-like fluid, which consists of dodecane, pyridine, quinaldine and heptylamine, adsorbed on a silica surface with supercritical $CO_2$ injection. Finally, the most complex approach was used by Sedghi et al. [11], where they correlated SARA fractions and the relevant gas chromatography

to come up with a complex mixture that best represented the oil type they planned to study (**Figure 1.6**).

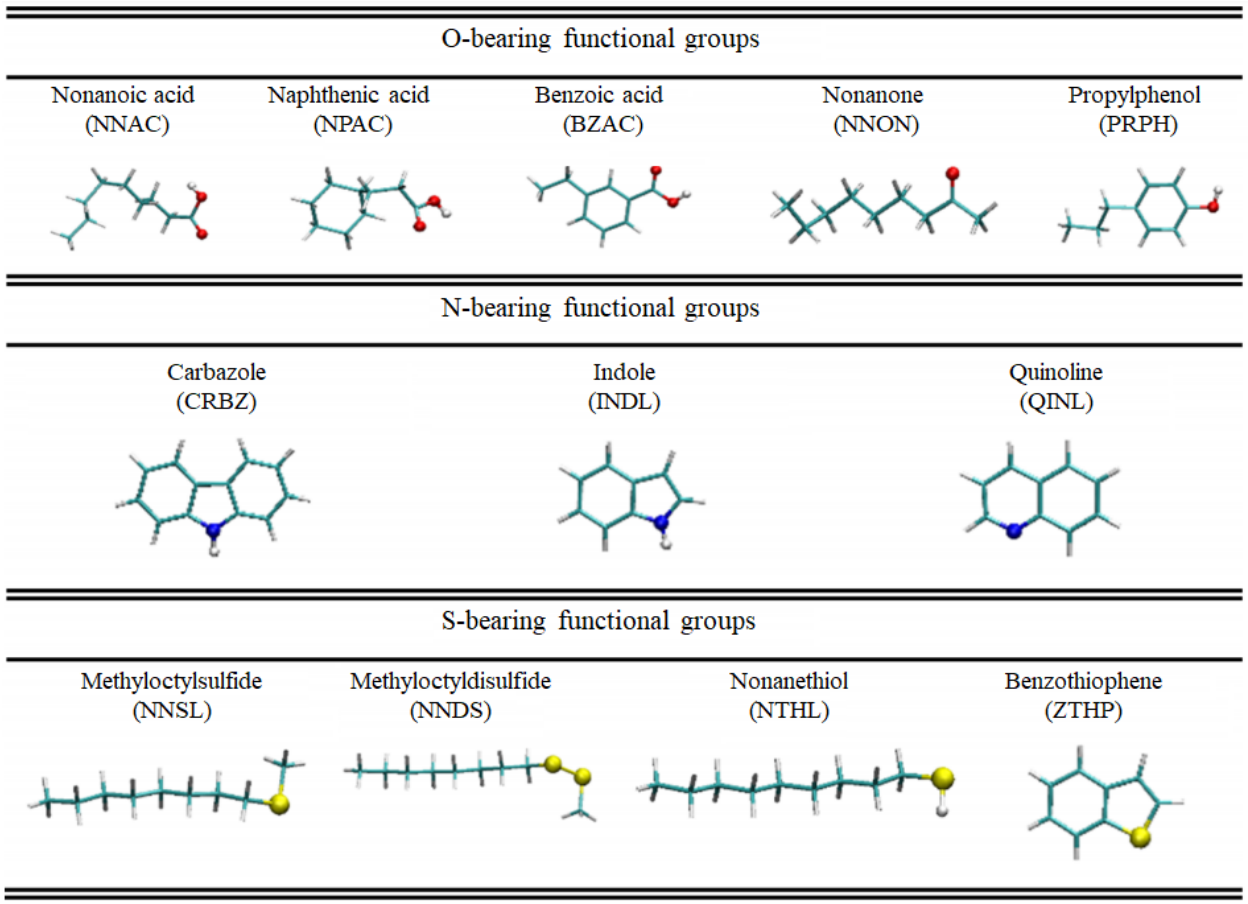


**Figure 1.6:** Oil molecules from SARA fractions and gas chromatography [11].

### 1.2.3.2. Injection gas

Hydraulic fracturing is one of the main technologies that allowed the exploration of tight and shale reservoirs. The most common fracturing fluid is water (more on this in the next section) and $CO_2$, however, $N_2$ and methane are becoming popular as alternatives. The simulation

parameters used for $CO_2$ simulation is mostly referred to as EPM2 model, which has reproduced supercritical point, the most common condition where $CO_2$ is injected [19]. Wu et al. [9] studied the displacement of methane by $CO_2$ and $N_2$ on a graphene nanopore, and they discovered that even though the adsorption of $N_2$ is lower than $CO_2$, it decreases the partial pressure of methane and consequently the displacement occurs. Methane has been used as injection fluid by Fang et al. [10] to successfully study the transport mechanism of this gas through water-filled pores. He used TraPPe FF, which is commonly used to represent methane since it correctly represents methane thermodynamics properties.

**1.2.3.3. Aqueous Phase**.

The aqueous phase has different roles in petroleum reservoirs and consequently in MD simulations. It has been used as solvent [38], displaced [12], and displacing fluid [16]. Most commonly, water ($H_2O$) is the only component of the aqueous phase, but some studies added ion to the solution (to simulate salts), while others have surfactants in the phase. When the effect of salinity [18, 26] is studied, $Na^+$, $Cl^-$, and/or $CA^{2+}$ ion are added to the water, and the conclusion was that the increased salinity would increase water/oil interfacial tension, while it has no effect on the contact angle [18]. On the other hand, when surfactants molecules are present in the aqueous phase, both contact angle and interfacial tension considerably decreased, which is also consistent with experimental results.

Different models and force fields have been used to represent water. The most common ones are: simple point charge (SPC), extended simple point charge (SPC/E, by far the most widely used approach in MD reservoir simulation [2, 3, 5, 8, 10, 20, 22], and three point (TIP3P) and four point (TIP4P-2005, the second most widely used model) transferable intermolecular potentials. SPC/E is widely used because it considerably speeds up the simulations because of its simplicity,

and can mimic experimental data [22] (**Table 1.1**). However, some researchers stated that TIP4P can better represent water/$CO_2$ IFT, and it matches experimental results at high pressures and temperatures [26]. Although there are many studies on water interaction with solids, neither of them investigated drainage/imbibition, or adsorption behavior of fluids when there is a thin water film adsorbed on the solid surface prior to the simulation. This is an important phenomena that does happen in oil reservoirs, and may drastically influence the phase behavior and transport of molecules.

**Table 1.1:** Force field parameters and electrostatic properties of common water models [35].

| Model | qO (e) | qH (e) | C6 (kJ mol-1 nm -6) | C12 (kJ mol-1 nm -12) | Dipole (Debye) |
|---|---|---|---|---|---|
| SPC | -0.82 | 0.41 | 2.6171E-03 | 2.6331E-06 | 2.27 |
| SPC/E | -0.84 | 0.42 | 2.6171E-03 | 2.6331E-06 | 2.39 |
| TIP3P | -0.83 | 0.41 | 2.4889E-03 | 2.4352E-06 | 2.35 |
| TIP4P | -1.04 | 0.52 | 2.5543E-03 | 2.5145E-06 | 2.18 |

### 1.2.4. Wettability Alteration

Wettability is the propensity of a solid surface to be preferentially wet by a fluid in the presence of another immiscible fluid [12]. This property is elementally related to the fluid adsorption on minerals of a pore space, and influences contact angle, interfacial tension, threshold capillary pressure, and fluid flow behavior. Researchers have used different approaches to model and represent this rock-fluid interaction property. The first, and the simplest, is to alter the interaction energy of walls made out of LJ particles, where one can make this parameter higher for polar, water-wet behavior, or nonpolar, oil-wet rock types [12]. The second is to alter the surface

functional groups, where users can change the hydroxyl groups (-OH), with a more polar attraction, to only hydrogen (-H), which makes it less polar. The third, and more sophisticated one, is to introduce surfactants on the medium. These compounds are known to alter the wettability of a surface because of their unique structure, where they have a lipophilic tail and a hydrophilic head.

### 1.3. Measurements

In this section we review a few research studies on the molecular dynamics of rock-fluid systems, with a focus on measuring macroscopic properties of the system such as density and diffusion coefficient and microscopic properties such as interaction energy.

#### 1.3.1. Density

Density is one of the most important parameter for molecular simulation of geological resources since it is used as an input as well as an output. In order to regulate the pressure in which the simulation system is going to be subjected, studies often use reference density of the fluid system at a given pressure from experimental data, such as the ones available at the National Institute of Standards and Technology (NIST) [41] After acquiring the density, then the number of molecules in the system can be calculated since the volume of the system is also an input. This approach has been used for $CO_2$ sequestration [18] and adsorption of nano-confined methane studies [23].

As an output parameter of the simulation system, density can also be applied to identify adsorption. Mass density is the amount of mass per volume, and in MD this mass can be measured by the sum of atoms in a given volume of the simulation box. To identify adsorption, studies observe the overall distribution of atoms/molecules through the simulation cell. If the

concentration of atoms/molecules of a given fluid is higher near the studied surface, the conclusion is that those molecules are adsorbed to the surface. Similarly, if the concentration of fluid molecules near the surface have reduced from the initial configuration, a desorption event occurred. This approach have been used in simulations involving alkane molecules associated with quartz [14], carbon [9], mica [10], and calcite [20] surfaces and $CO_2$ with carbon, and calcite as well as water in shale inorganic and organic matter [27].

The monitor of density, as a distribution of molecules through the system, has been also used to assist contact angles (CA) measurements. In summary, CA is the angle formed between two non-miscible fluid phases and a surface, and it is measured in relation to the denser phase. CA is mostly used to identify wetting behavior of the solid. Basically, if a CA is lower than 90° implies that the denser fluid phase preferentially wet the surface. Since usually water in present on the medium and it is often the denser phase, it is common to refer to surfaces as water-wet or oil-wet. Since it is hard to visually differentiate molecules in a simulation cell, density has been use as a mechanism to identify molecules distribution. This approach has been used to calculate contact angles on quartz [18, 26], mica [10], and to monitor wettability alteration in organosilanes [12].

### 1.3.2. Interaction Energy

An important parameter to study and explain the behavior of molecules and its fluctuation through the simulation box is the interaction energy. This parameter predicts how likely an atom/molecule would attract or repel other atoms/molecules. In MD simulation this energy is calculated every step for all molecules by the so called non-bonded interactions, which is the sum of electrostatic and mechanical, or van Der Waal's interactions. The former is mainly calculated

using Coulomb's law, while the latter employs Leonard-Jones potential (a better description of bonded and non-bonded interactions is detailed in Methods section).

In a force field, each atom is intrinsic described by a partial charge, applied to calculate electrostatic energy interaction, the collision diameter and well depth, which are both necessary to calculate Leonard-Jones potential. For molecules where the partial charges are significant, molecules that create poles, also known as polar molecules, the electrostatic is much higher than the mechanical interaction. On the other hand, for neutral molecules or nonpolar molecules, the van der Waal's interactions are taken in account. For instance, a quartz surface, composed by $SiO_2$, when described by the CLAYFF [34] or CVFF [6] force field is highly charged, which explain its behavior of preferentially attracting and adsorbing polar molecules such as water over nonpolar hydrocarbon molecules [6, 21]. On the other hand, an organic shale surface is usually represented as (or by) graphite, which is composed of carbons with zero partial charge in the OPLS force field, greatly adsorbs nonpolar hydrocarbons molecules [8, 17, 25].

## 2. Molecular Dynamics Simulation of Hydrocarbon Mixture in Shale Nano-pores

### 2.1. Introduction

The depletion of conventional oil reservoirs forced companies and consequently researches to pursue alternatives in reservoirs that in the past were considered not being economically viable. The consequential advance in drilling and well completing technologies, mainly horizontal drilling and hydraulic fracturing respectively, enabled the exploration of these "unconventional" reserves. However, the unusual high temperatures and pressures, have increased the cost as well as the hazardous level for reservoir analyzes by lab experiments. In addition, the complicated nanopore rock structure, that may influence phase behavior of fluids, can effect standard reservoir simulation equations, such as oil in place (OIP) prediction. Molecular Dynamics (MD) simulation has been proved to be an important inexpensive tool to replicate reservoir pore and fluid conditions, as well as to monitor fluid behavior as demonstrated in Chapter 1.

Unconventional reservoirs characteristics include a low porosity, not always the case, but mainly low permeability medium. Some examples are source rocks, and coal bed methane. The former, as the name suggests, are rocks, most commonly shale, which generates petroleum by the maturation of the organic matter, such as kerogen, present in them. The latter is composed of an organic rich matter that underwent an extreme process of maturation, under high pressures and temperatures, which resulted in an organic pore matrix, coal, and light hydrocarbons, methane. The pressures in which these reservoirs are normally encountered are extremely high, and allied to the fine particles deposition environment they were generated, resulted in pores in the nanometer scale, in contrast to the millimeter or micrometer scale for conventional reservoirs.

Previous MD studies have used graphite as a model to simulate the organic pore matrix that is common to these rocks.

Even though reservoir fluids and pores interactions have been studied using MD simulation, the pores either used simplistic pore crystal structure, pore geometry or fluid composition. Welch et al., [24] observed the retrograded condensation of a 70/30 weight % of ethane/heptane hydrocarbon mixture at bulk phase, but they could not observe the phase transition at an atomistic crystal nanopore. Zhong et al., [21] analyzed the adsorption mechanism and preference on a silica surface, but they only studied the influence on a single slab of surface, so he underestimated the effect of pore vertices. Ambrose et al, [25] calculated the mass density increase at the surface walls of a graphite nanopore, but he used a slit-pore model that does not account the effect of a full-walled pore. Wu et al., [7] detected the effect of wettability on hydrocarbon accumulation on an organic shale pore, but they only used a single surface slab to study. Sedghi et al., [11] studied the oil displacement by brine in an atomistic calcite nanopore, but the used force field was not parametrized for the atoms connections at the pore vertices. Sedghi et al., [12] observed the formation of oil-layer after water injection, but he used a simplistic Leonard-Jones model.

Here, a Molecular Dynamics study of nanoconfinement effect on hydrocarbon fluid phase and compositional behavior in organic shale rocks is presented. The pore is modeled by a fully atomistic squared graphite pore that satisfies all the requirements of the force field in use. This pore accounts for the total effect of wall surfaces, and vertices effects. The model have the capacity to simulate a more oil-wet or water-wet behavior by manipulation of radicals on the surface. The hydrocarbon fluid mixture is composed by a 70/30 weight % of ethane and heptane respectively. The system is subjected to reservoir temperatures and pressures, and the outputs are analyzed by

density and compositional variation through the simulation box to observe phase behavior. Simulations include hydrocarbon fluid mixture at bulk and nanopore conditions, hydrocarbon migration and accumulation, spontaneous imbibition and drainage, and water injection.

## 2.2. Methods

In this section all the simulation models, parameters, and programs used in this study are presented. Firstly, we discuss how molecular dynamics (MD) simulations are performed. MD is the time dependent behavior of molecules under a force-field. The molecules motion inside the simulated box is dependent on the Newton's second law of motion:

$$F = ma$$

where $F$ is force, $m$ is mass, and $a$ is acceleration. The derivation of velocity ($v$) over time (t) is equal to acceleration, and by substituting in the equation above, the result is:

$$\frac{dv}{dt} = a \rightarrow \frac{dv}{dt} = \frac{F\,(x)}{m}$$

The velocity of the molecules, and consequently the motion of them between each time step, is then influenced by the forces that are applied to each atom in a molecule. In MD, the forces that affect each atom are a result of the negative gradient of the potential energy

The forces applied to each atom in a MD simulation are calculated as the negative gradient of the potential energy ($U$) of that atom.

$$F(x) = -\nabla U\,(x)$$

The potential energy is calculated for each time step during the simulation, and it is essentially based on the sum of non-bonded and bonded interactions. The bonded interactions include the energy generated by bonds stretching, angles bending, and dihedrals torsion potentials. The non-bonded interactions are categorized as mechanical and electrostatic interactions. The electrostatic interactions are calculated using the Coulomb's law equation, which is depicted below:

$$v^{Coulomb}(r) = \frac{Q_1 Q_2}{4\pi\epsilon_0 r}$$

where $r$ is distance between atoms, $\epsilon_0$ is the vacuum permittivity, and $Q$ is the charge of the atoms involved in the interaction. The mechanical interactions, or van der Waals interactions, are computed applying the Leonard Jones potential equation:

$$v^{LJ}(r) = 4\varepsilon\,[\left(\frac{\sigma}{r}\right)^{12} - \left(\frac{\sigma}{r}\right)^{6}]$$

where $\varepsilon$ is the well depth, and σ is the distance between the involved atoms in which the potential is zero. Each atom receives a specific value for all the parameters, which appear in the equations above, and they differ from force field to force field. These parameters in the force-fields were acquired by either ab-initio molecular dynamics simulations, or experiments [34, 35]. In the next sections, the force-field choice, simulation models, and setup are exhibited.

### 2.2.1. Simulation Details

All the simulations in this study were performed utilizing Gromacs simulation tool [42, 43]. OPLS-AA [44] force-field was used to represent both pore and hydrocarbon molecules, and water was represented by the SPC/E [35] model. To calculate van der Waals interactions, Verlet

algorithm [45] with a 1.5 nm cut-off distance was applied. For long range electrostatics interactions, past cut-off distance, the Particle Mesh Ewald (PME) algorithm [46] was employed. All simulations were performed under a NVT (constant number of atoms, volume, and temperature), where the temperature controlled by the V-rescale thermostat, a modified Berendsen thermostat, with a 0.2 fs. The simulations were run for at least 5 ns, which results in a total of 2,500,000 time steps. The output of the simulations were analyzed by in-house Fortran codes, and the visualization was performed by VMD [47].

### 2.2.2. Pore Model Details

Few previous studies have implemented pores with irregular cross sections (non-circular and not a slit-pore) [11]. When they did, the pore walls connections at the vertices can be considered unnatural since the force field they used did not account for these bonds on its parametrization. Here we present a simulation of a fully atomistic squared organic shale pore that fully satisfies all the requirements of the force field in use, and that correctly describes bonds at the vertices. The fluid in the pores is a mixture of 70 weight % ethane and 30 weight % heptane. The organic shale pore was based on a graphite rock. Graphite essentially consists of compact layers of graphene, which have an average of 0.335 nm space in between. The graphene sheet model can be seen in **Figure 2.1**. This model consists of a layer of $sp^2$ bonded carbons arranged on a hexagonal lattice, much like a honey bee panel. Then, an in-house Fortran code was utilized to remove all the atoms and bonds in the desired radius from the center of the sheet. The carbon dangling bonds were then

connected to hydrogen (-H) (**Figure 2.1a**), creating a desired more oil-wet surface, or a hydroxyl (-OH) (**Figure 2.1b**), which results in a surface with a water-wet behavior.

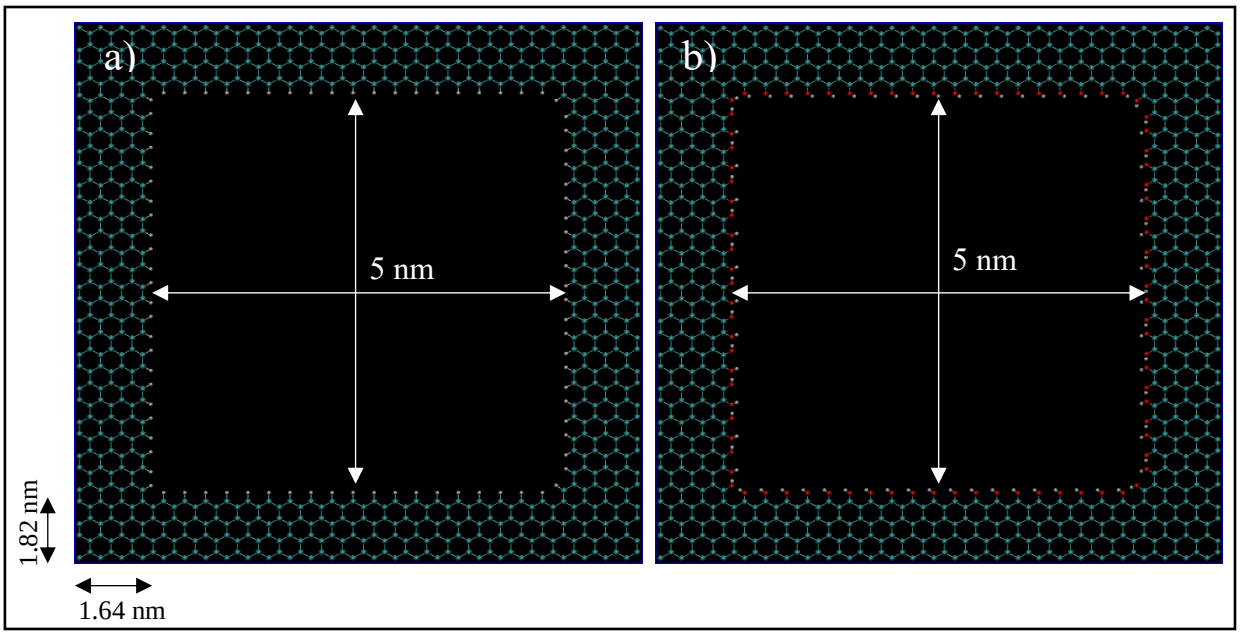


**Figure 2.1:** Graphene sheet structure. The dangling bonds were connected to (-H), a), or (-OH) b). Cyan, white, red spheres are carbon, hydrogen, and oxygen atoms respectively.

In this study, two pore models were implemented. The first one, shown in **Figure 2.2a**, consists of a 16 stacked sheets of graphene, 0.335 nm apart, which results in a 5.36 nm long pore. The pore model has a 5 x 5 $nm^2$ squared cross-section. The pore walls are 1.64 nm and 1.82 nm in x and y directions respectively, which is higher than the 1.5 nm cut-off distance. The pore was then placed at the middle of the simulation box, and a total volume of 6.64 x 6.82 x 30 $nm^3$ (15 nm in each side) was designated to be filled by the fluid molecules. The second one, shown in **Figure 2.2b**, consists of two connected pores. Model two incorporated model one by connecting it to a 2 x 2 $nm^2$ squared cross-section pore, which was constructed similarly to the 5 nm pore. The connected pores where then placed at the left side of the simulation box and the 2 nm end that

interacts with the bulk phase was blocked. This way the molecules that would interact with this pore could only come from the 5 nm pore. Then a total volume of 6.64 x 6.82 x 30 $nm^3$ was left as void space to be filled by fluid molecules.

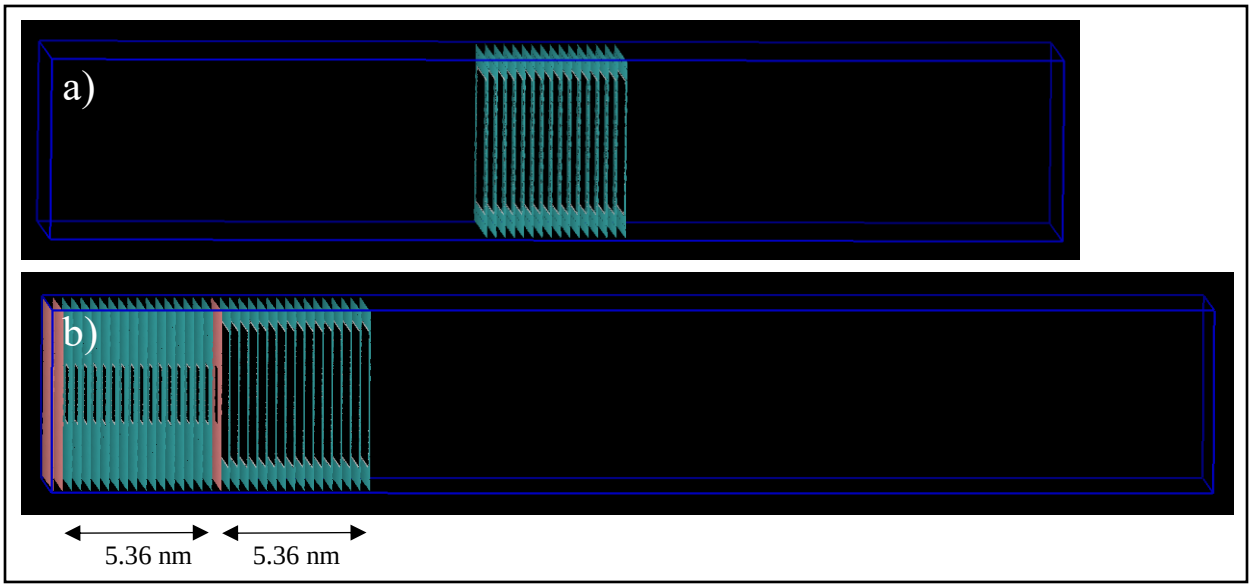


**Figure 2.2:** Pore simulation box. a) Single pore, and b) connected 5 nm to 2 nm squared pore models. Cyan and white spheres are carbon and hydrogen atoms respectively.

## 2.3. Results and Discussion

### 2.3.1. Mass Transfer

In this section, the mass density of single component, and a mixture of fluids is monitored for the case of a 5 nm single pore. The idea is to observe the ability of MD simulations to replicate phase characteristics in the bulk, and to account for the nanoconfinement effect when a pore is introduced to the system. The fluids are tested in three temperature and pressure conditions, where condition 1 (C1) is gas phase, condition (C2) is two phase, and condition 3 (C3) is liquid phase.

#### 2.3.1.1. Ethane Single Component

Ethane is a light hydrocarbon encountered in most light oil or gas reservoirs. Since unconventional reservoirs have high temperatures and pressures, this molecule has an even higher chance to appear due to cracking of heavier hydrocarbons or kerogen molecules. In this section, three different scenarios were studied: gas, biphasic (gas/liquid), and liquid phases. In order to represent these phases in a simulation, temperatures and pressures were acquired from the NIST webbook [40].

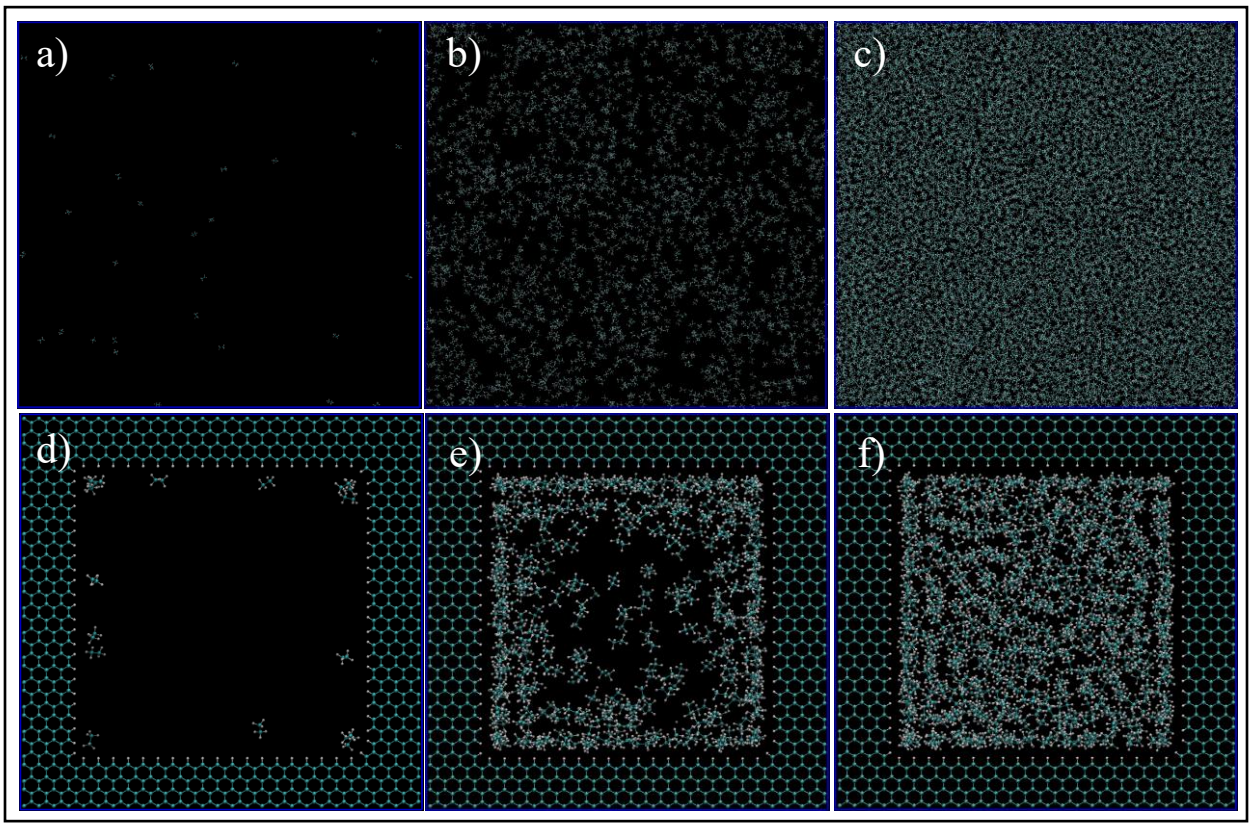


**Figure 2.3:** Ethane molecules simulation in bulk (a,b,c) and pore medium (d,e,f) at gas (a,d), two phases (b,e), and liquid (c,f) condition. Cyan and white spheres are carbon and hydrogen atoms respectively.

Firstly, we qualitatively analyze the results of the simulations by investigating the results given in **Figure 2.3**. For the gas phase (**Figures 2.3a** and **2.3d**, -68 °F, 14.7 psi), the bulk simulation box exhibits spaced out molecules as expected for the phase. However, for the confined pore box, all of the molecules inside the pore are accumulated adjacent to the walls, and the majority of them are close to the vertices. This later observation is interesting since it is possible to observe oil accumulations patterns, and is justifiable because there is a higher concentration of pore carbon atoms which then translates to higher van der Waals interactions, which can induce dipole- induced dipole, between the ethane and graphene. For the two phases case (**Figure 2.3b** and **2.3e**, -68 °F, 546.21 psi), the bulk simulation box shows a pattern of accumulated molecules and void spaces. Visually, this can mean that we have gas and liquid phases in our system. This trend is even more present in the confined pore space, where near the wall there is high accumulations of ethane, while in the center void space is predominant. The implications of this analysis can demonstrate that with nano-confinement, there is a presence of a liquid phase near the pore walls, while a gas phase flows inside the pore. For the liquid phase (**Figures 2.3c** and **2.3f**, - 68 °F, 4000 psi), there is almost no void space, so all of the molecules are close to each other, which is indeed the characteristics of liquid phase. The same trend can be observed in the pore confined space, but again higher accumulations of molecules can be observed near the pore walls.

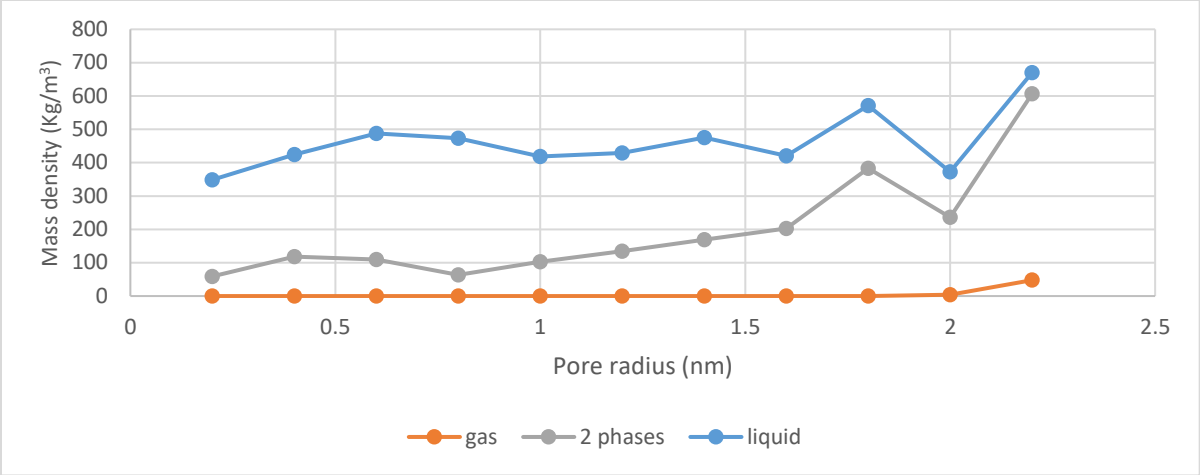


**Figure 2.4:** Ethane mass density over pore radius in gas, two phases and liquid conditions.

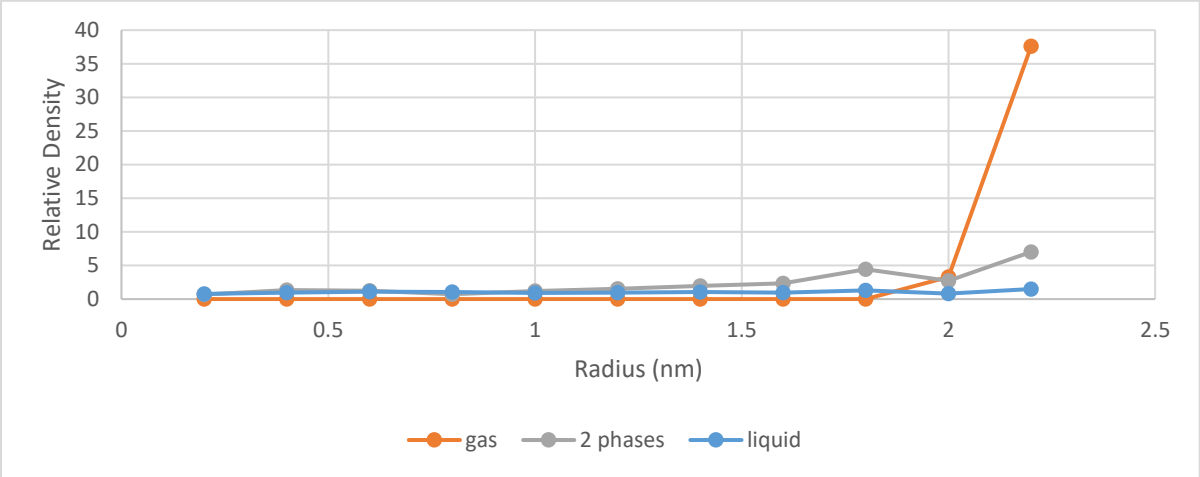


**Figure 2.5:** Ethane relative density (mass density inside the pore over the density of the phase in bulk conditions) over pores pore radius in gas, two phases and liquid conditions.

Qualitative analyses are important to introduce the subject and highlight the aspects that require deeper investigations. In order to do so, the density over the pore radius was calculated by developing and using an in-house Fortran code that identified the number of atoms alongside the area from the center to the pore walls. As shown in **Figure 2.4**, it can be observed that there is a lower density region at the center of the pore, while there is a high rise in the number of ethane molecules towards the pores walls. The highest density is observed at the walls, which is translated to adsorption. Another highlight is a second peak in the graph, which can represent a second

adsorption layer, a common trend that is also observed in experiments and prior simulations. Finally, in **Figure 2.5** relative density over the pores radius is analyzed for the three cases, and it can be observed that the gas phase is the one mostly affected by nano confinement, while the liquid phase is the least affected. This is an interesting observation, since it can be explained by the quantity of molecules present in the simulations, and also be related to experimental and previous simulations results, where the bulk phase is completely changed when the nano confinement is applied.

#### 2.3.1.2. Heptane Single Component

When compared to ethane, heptane is a heavier molecule that is mostly present in the liquid fraction of reservoir oils. In consequence of this fact, this component is encountered in a gas phase at a fewer range of pressures and temperatures in contrast to ethane. Furthermore, in order to simulate it at a gas condition, the temperature of the simulations had to be set at 248 °F. Even

though it is an elevated temperature, this setup is commonly found in unconventional reservoirs that are located at greater depths.

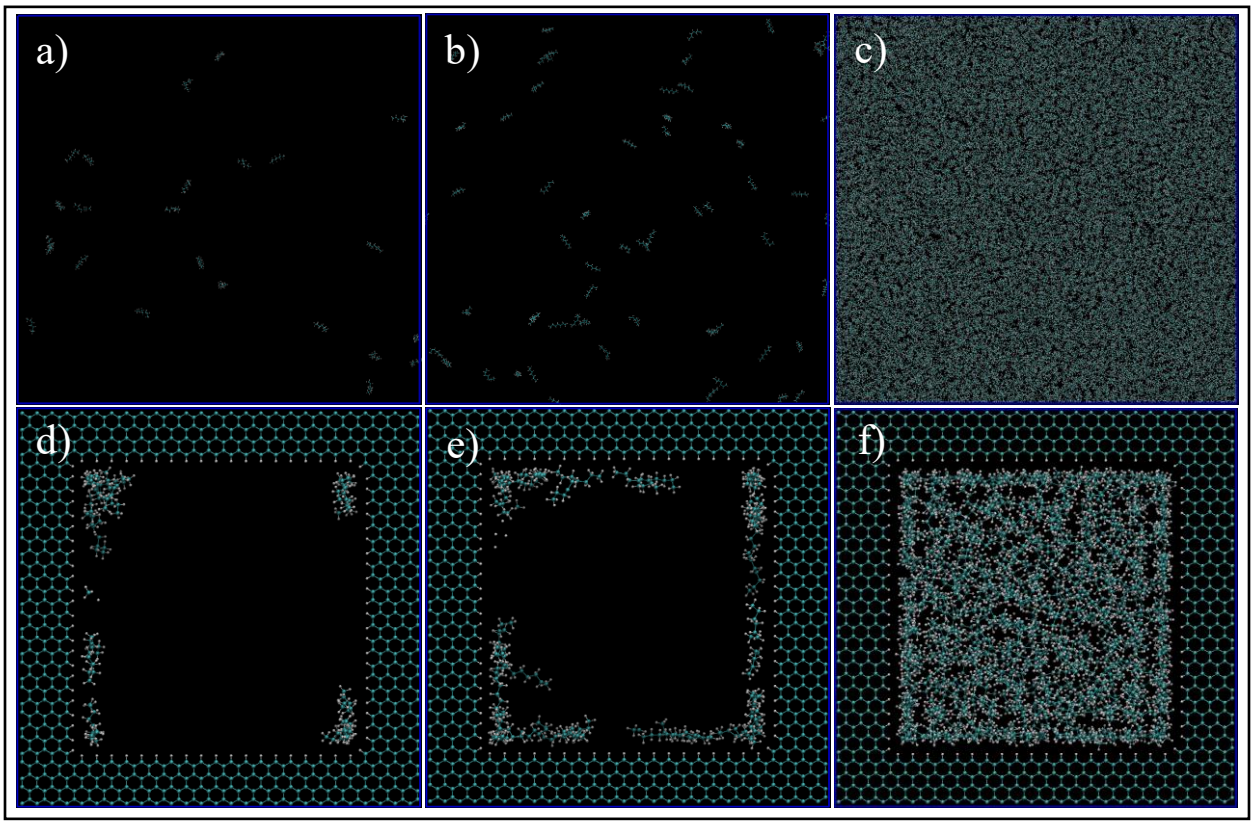


**Figure 2.6:** Heptane molecules simulation in bulk (a,b,c) and pore medium (d,e,f) at gas (a,d), two phases (b,e), and liquid (c,f) condition. Cyan and white spheres are carbon and hydrogen atoms respectively.

Again, three scenarios were studied in this section: gas, biphasic (gas/liquid), and liquid, and the pictures of the molecules at the end of simulations are shown in **Figure 2.6**. For the gas in bulk (**Figure 2.6a**, - 248 °F, 14.7 psi), the simulation box exhibits dispersed heptane molecules that move freely apart from each other, as expected for a gas phase. However, when a pore is introduced, heptane molecules migrated to the pores walls and their movement is restricted to this confined region, especially to the corners of the graphene pore. For the two phase mixture in bulk (**Figure 2.6b**, - 248 °F, 54.17 psi), heptane molecules are more agglomerated, and lumps of three

molecules can be seen moving in conjunction. Even though, this cannot be considered a liquid phase, it represents a more liquid-like behavior than the gas phase. At nano confinement conditions, the heptane molecules coat the pore surface, and again a higher accumulation of these molecules can be found at the corners of the pore. For the liquid in bulk (**Figure 2.6c**, - 248 °F, 4000 psi), a massive agglomeration of heptane molecules is encountered, and the molecules have limited space to move around since there is almost no void space. This representation is expected for liquid phases. When a pore is introduced (**Figure 2.6d, e** and **f**), a similar trend is observed, but in this case a higher concentration of molecules is encountered near the walls. Similar to ethane, the molecules preferentially located near the walls, which represents an adsorption behavior.

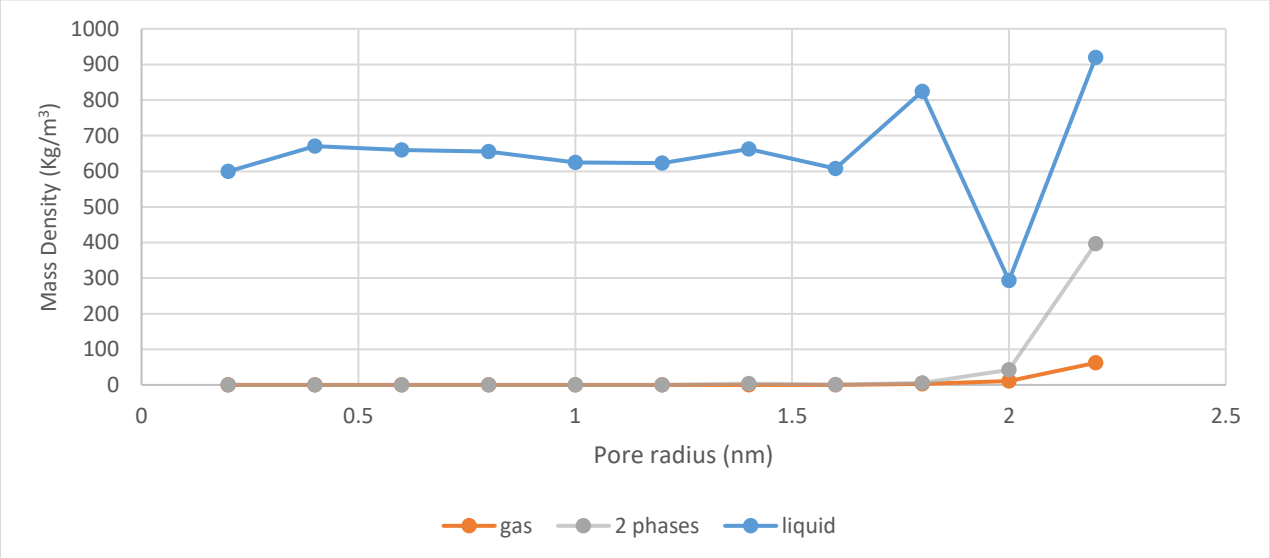


**Figure 2.7:** Heptane mass density over pore radius in gas, two phases and liquid conditions.

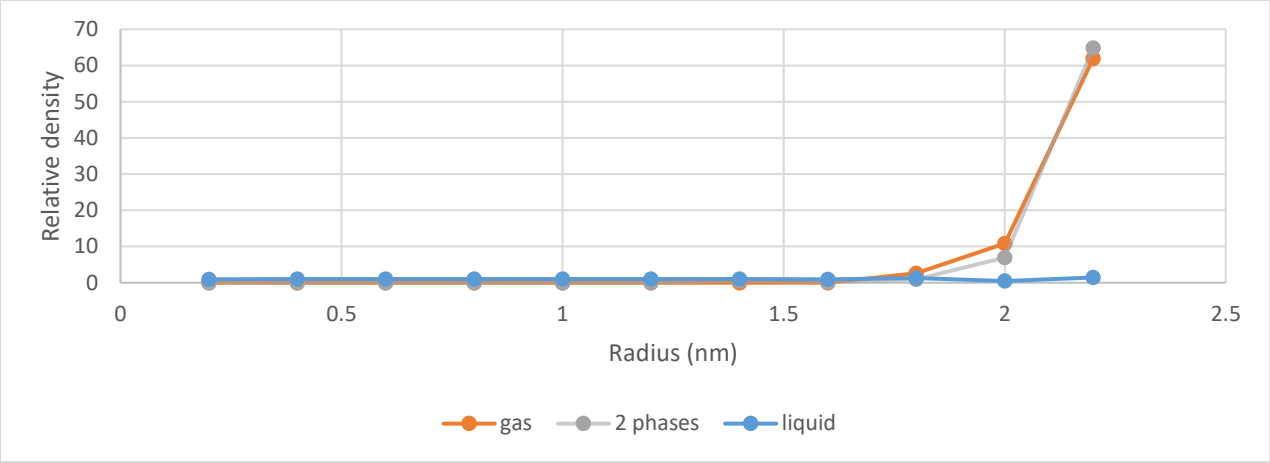


**Figure 2.8:** Ethane relative density (mass density inside the pore over the density of the phase in bulk conditions) over pores pore radius in gas, two phases and liquid conditions.

Performing a quantitative analysis, we can see in **Figure 2.7** how the heptane molecules are distributed over the pore radius. Following the same trend line as the ethane simulation, there is a higher concentration when the radius is closer to the pore walls, which results in a higher density of the phase. This observation can also be interpreted as an adsorption of heptane molecules to the graphene wall, which emphasizes what was seen in previous figures. Since only nonpolar molecules are involved, the mechanism of adsorption can be again explained by the van der Waals interactions, induced dipole – induced dipole, between the oil molecules and pore walls. Another interesting observation is a drop and a subsequent peak in density, which implies a second layer of adsorption, and it is present in previous simulations and experiments. **Figure 2.8** reveals the effect of nano-confinement in each simulated phase for heptane. Since the two phase and gas phase had similar pressures, they were the ones mostly affected when the pore was introduced to the system. This behavior can be explained by the lower pressure that the molecules are subjected to, which implies less restriction to movement. The molecules can then interact with pore walls more freely compared to liquid phase simulation.

This set of simulations (single component cases) were important to make sure that our simulation approach is appropriate to model molecules behavior in different phase with and without pore nano confinement effects.

#### 2.3.1.3. Ethane/Heptane Mixture

Reservoir oils are rarely composed on only one component, so in order to simulate a more realistic fluid, a mixture of heptane and ethane was studied. The mixture is composed of 70% ethane and 30% heptane from the total weight. These fractions were chosen to better represent unconventional oil. These type of reservoir oils are normally subjected to elevated temperatures and pressures, which induces cracking of heavier molecules into lighter ones, which explain the choice for a higher weight percent of ethane. However, since one of the goals of this study was to analyze phase transition in a mixture, it was necessary to introduce a heavier molecule, heptane, which is also normally encountered in unconventional reservoirs.

A total of six simulations were executed to observe the gas, 2-phase (liquid and gas), and liquid phases at bulk and confined pore conditions. The temperatures and pressures for these phases were acquired from a code created in our research group, which essentially implements the Peng-Robinson equation of state to analyze phase behavior of hydrocarbon mixtures.

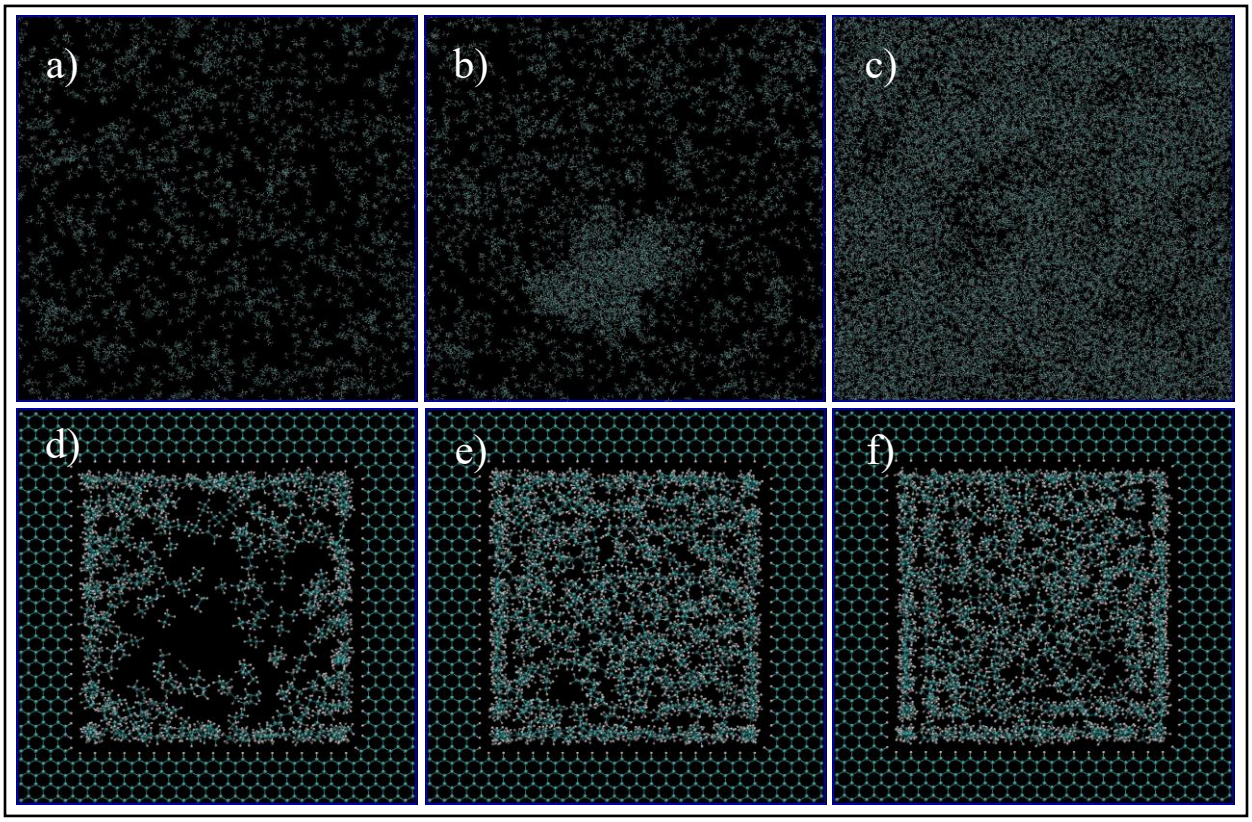


**Figure 2.9:** Ethane/Heptane mixture simulation in bulk (a,b,c) and pore medium (d,e,f) at gas (a,d), two phases (b,e), and liquid (c,f) condition. Cyan and white spheres are carbon and hydrogen atoms respectively.

**Figure 2.9** exhibits images at the end of each simulation that are used for a qualitatively analyzes. For the gas phase in bulk (**Figure 2.9a** and **2.9d**, 260 °F, 300 psi) shows molecules dispersed in the medium, and they move freely through the simulation box. However, when the system is subjected to a pore medium, the molecules migrate inside the pore and accumulate mostly at the pore walls, with a higher concentration at the corners. The molecules near the walls have restricted movement, opposed to molecules at the center of the pore, which is also visually mostly composed of ethane. With these observations, it is possible to infer that molecules near the wall have a liquid

like behavior while the ones at the center have a gas like conduct. For the liquid phase (**Figure 2.9c** and **2.9f**, 68 °F, 700 psi), the molecules are encountered in a high level of agglomeration and dense medium, and their slight movements are restricted to the movement of adjacent molecules. For the pore simulation of this phase, the behavior of molecules are similar to the gas phase, but the only difference is the high concentration of molecules at the center of the pore, which is expected because of the initial imposed liquid phase conditions. For the two phases in bulk (**Figure 2.9b** and **2.9e**, 150 °F, 600 psi), two distinct behaviors for the molecules were observed, one were the molecules being dispersed and moving freely, similar to the gas setup simulation, and second were the molecules being located on a condensed cluster moving relative to its adjacent molecules, similar to the liquid setup simulation. For the pore simulation, the behavior of the molecules is similar to the liquid phase. This observation implies that the Peng-Robinson equation of state code and simulations on this section are in concordance when representing the different phases of this mixture.

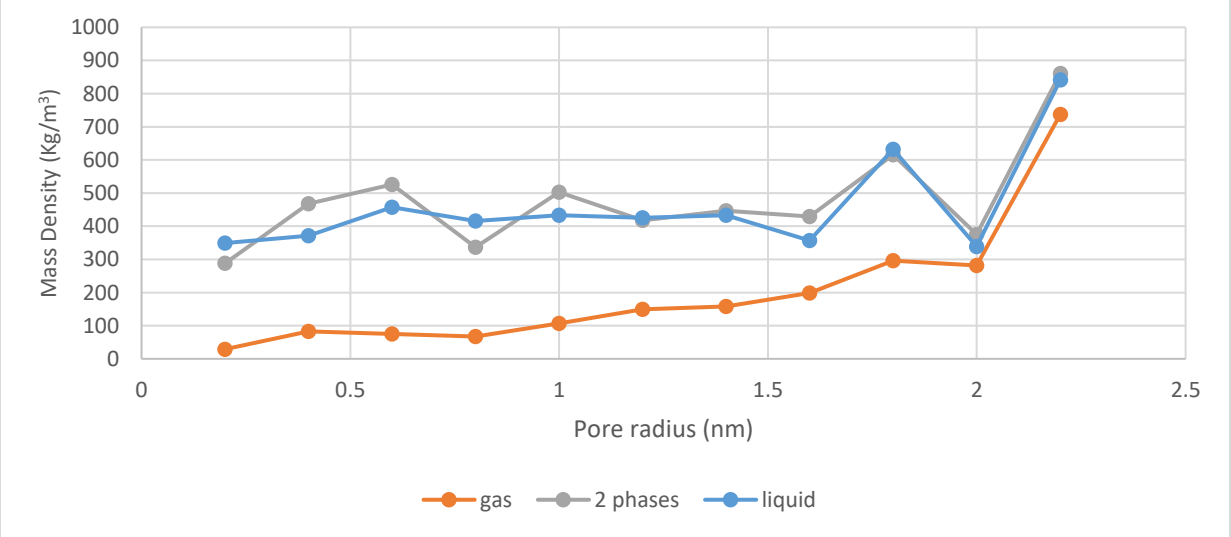


**Figure 2.10:** Mass density over pore radius in gas, two phases and liquid conditions.

Following up with the analysis on this section, the results of the mixture simulation were quantitatively investigated, and the outcome is shown on **Figure 2.10**. This figure shows a graph with the variation of mass density over the pore radius. A similar trend is seen for all three setups, where a lower density is observed at the center of the pore and it reaches a peak when it is the closest to the pore wall. This peak can be recognized as a layer of adsorption on the wall since this region has a higher intermolecular interaction energy with the oil molecules. A second observation of this graph, which is also seen in previous pore simulations, is a depression in the graph followed up by a second peak in relative density. This phenomena is also seen previously, and it represents the second layer of adsorption.

### 2.3.2. Hydrocarbon Mixture Composition Alteration

In previous sections, the effect of nano-confinement on mass transfer from bulk to pore has been identified, but this phenomena also influences the composition of the fluids. In previous studies, when pore effect is taken in account, such as capillary pressure, the fluid composition inside nanopores and in bulk does differ [49]. In addition, there is a tendency of increase in heavier molecules composition in nanopores [49]. In order to observe and study this phenomena, three simulations were performed, one for each fluid mixture condition, and the behavior of heptane, here the heavy molecule, and ethane molecules were analyzed by pictures and mole fraction variation though the box and inside the pore.

Initially, the movement of hydrocarbon molecules was analyzed for the whole bulk-pore system. The initial and final configurations of the system is shown in **Figure 2.11**. For all cases, it is possible to observe an increase in the number of heptane molecules, yellow, inside the nanopore, in detriment to its number in the bulk. In order to assist and confirm this visual observation, the heptane mass fraction in pore and bulk was acquired and the results can be seen in **Table 2.1**. Firstly, even though the molecules were placed randomly inside the pore, the initial mass fraction of heptane is near to the desired value of 30% for all mediums and conditions. Secondly, the mass fraction of this heavier molecule increases for the pore medium for all conditions, while it decreases in the bulk medium. This inference reinforces the results from the visual observation explained next.

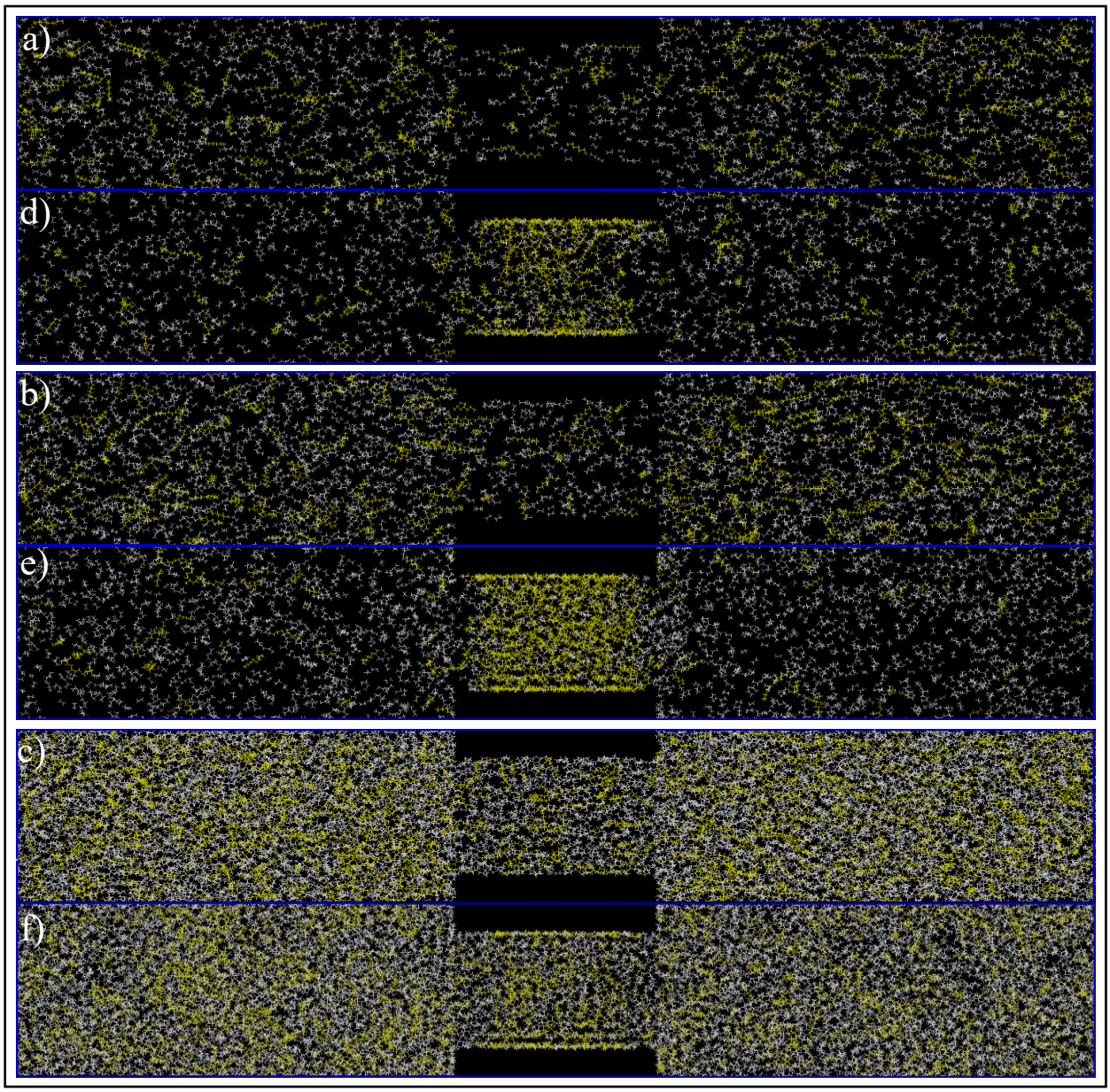


**Figure 2.11:** Initial (a, b, c) and final configuration (c, d, e) of ethane/heptane mixture at gas (a, d), two phases (b, e) and liquid (c, f) conditions. Yellow and white colors are heptane and ethane molecules respectively.

**Table 2.1: Initial and final heptane mass fraction in bulk and pore mediums.**

| Condition | Bulk - Initial $C_7H_{16}$ mass fraction | Pore - Initial $C_7H_{16}$ mass fraction | Bulk - Final $C_7H_{16}$ mass fraction | Pore - Final $C_7H_{16}$ mass fraction |
|---|---|---|---|---|
| C1 | 0.3206 | 0.3447 | 0.2411 | 0.5087 |
| C2 | 0.3052 | 0.2858 | 0.1301 | 0.6991 |
| C3 | 0.3147 | 0.2658 | 0.3068 | 0.3967 |

Next, a detailed assessment of hydrocarbon molecules mass transfer inside the pore was performed. Images at the entrance of the pore can be seen in **Figure 2.12**. For all conditions, increased concentration of heptane in the pore is noted. As it can be seen, Heptane concentration increases from the center of the pore, to the pore walls, where there is predominant yellow color. To investigate this latter observation, the radial mass fraction of heptane was calculated and plotted, as shown in **Figure 2.13**. The mole fraction of the heavier hydrocarbon molecules increases radially, and it is at the maximum value closest to the wall. Again, the mole fraction analysis is in concordance to the visual assessments of the molecules.

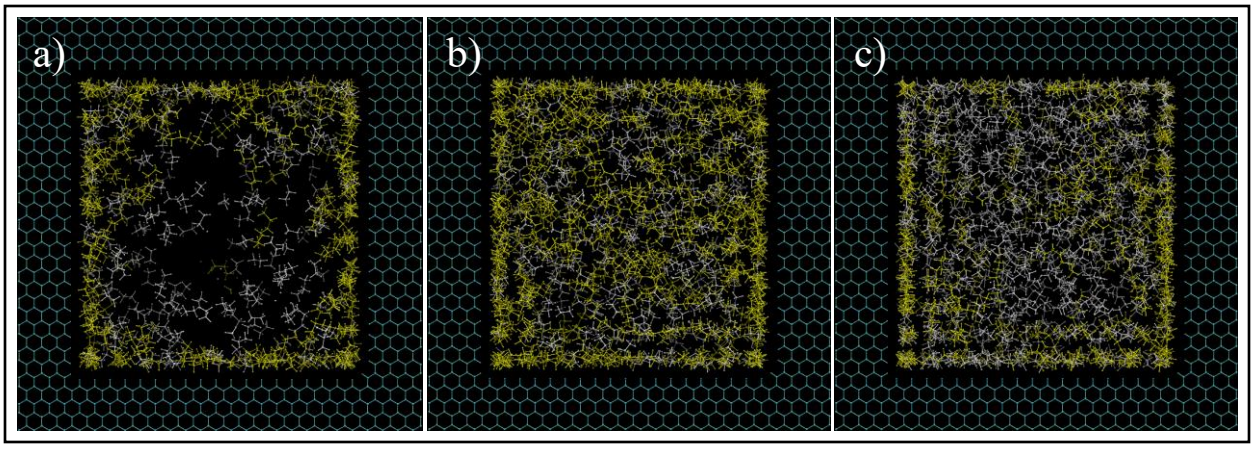


**Figure 2.12:** Images at the pore entrance of gas (a), two phases (b) and liquid (c) conditions simulations. Yellow and white colors are heptane and ethane molecules respectively.

Finally, it is important to understand the mechanism behind the hydrocarbons molecules movement and consequently composition change. In this section, in concordance to previous studies, the fluid composition did change in all conditions, and there is a tendency of increase in mass fraction of the heavier component, in this case heptane, and decrease in the lighter component, ethane. This later observation can be explained by the van der Waals interaction between the pore and hydrocarbons. Since hydrocarbon and pore atoms can be considered non-polar molecules, their interaction are in the type of induced dipole – induced dipole. Since heptane molecule has a longer chain compared to ethane, it is easier for an induced dipole to form, and consequently these heavier molecules would have a higher interaction energy with the solid surface. This explains the motion of heptane molecules to the pore, and its preference to be located at the closest to the pore walls. Although, the trends observed here for composition change from bulk to pore and pore center to pore walls, are present in all conditions, they are more predominant to the gas and two phase condition, especially to the latter one. For condition 2, heptane demonstrated the highest heptane mass composition increase in the pore when comparing initial

and final configurations, and it achieved the highest composition peak compared to other conditions, at the pore walls. This behavior can be explained by the capillary effect. Surfaces are usually preferentially being wet by liquids over gas [48]. Since in Condition 2, gas and liquid are present, the pore surface preferentially adsorbs the liquid phase, and since the liquid phase is mostly composed by heptane, the concentration of heptane molecules increases more efficiently than the other conditions. This behavior was also observed in a research study by Zhang et al. [49] from my research group. In this study, they noted that heavier molecules tend to migrate from the bulk (fracture) to the matrix (nano-pore).

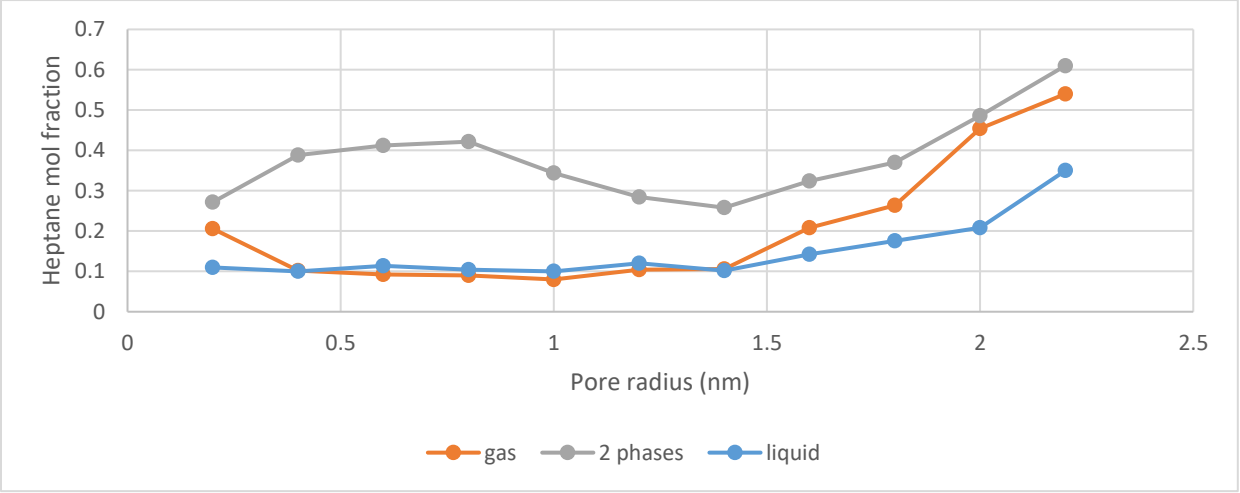


**Figure 2.13:** Relative density (mass density inside the pore over the density of the phase in bulk conditions) over pores pore radius in gas, two phases and liquid conditions.

Next, we quantitatively analyze the distribution of ethane and heptane in the graphite nanopore. As shown in **Figure 2.12**, in the nanopore that is in the middle, the heavier molecules, e.g. heptane (yellow color) tends to adsorb to the graphite wall while ethane molecules (white color) accumulate at the center (also shown in **Figure 2.13**). One other observation is that the heavier molecules migrate from the two large side pores to the nanopore in the middle, and eventually, the overall concentration of the mixture in the nanopore changes from its initial value

of (70%-30%) ethane-heptane to nearly 50%-50% ethane-heptane (see **Table 2.1** for the values). These results suggest that the overall composition of the system does change when the fluid interacts with the pore and the overall density of the mixture increases radially from the center to the pore wall. Heptane, which is here the heavier molecule, preferentially interacts/adsorbs on the surface of the wall since they have greater van der Waals forces and longer chain.

### 2.3.3. Connected Nano-Pores

In the previous sections, mass transfer and composition alteration has been studied for a setup with the bulk phase in contact to a 5 nm cube-shaped pore. However, considering that shale rocks are heterogeneous in terms of pore size, it is relevant to analyze how these parameters behave when a 2 nm pore is introduced, which would represent two connected nanopores with different sizes. To do so, three simulations, with the same three phase conditions of the same ethane/heptane mixture, in a system with a bulk medium in contact to two connected pores, 5 nm and 2 nm in sequence, were performed. In this section, the mass density and composition alteration of the above described system was studied.

### 2.3.3.1. Mass Transfer

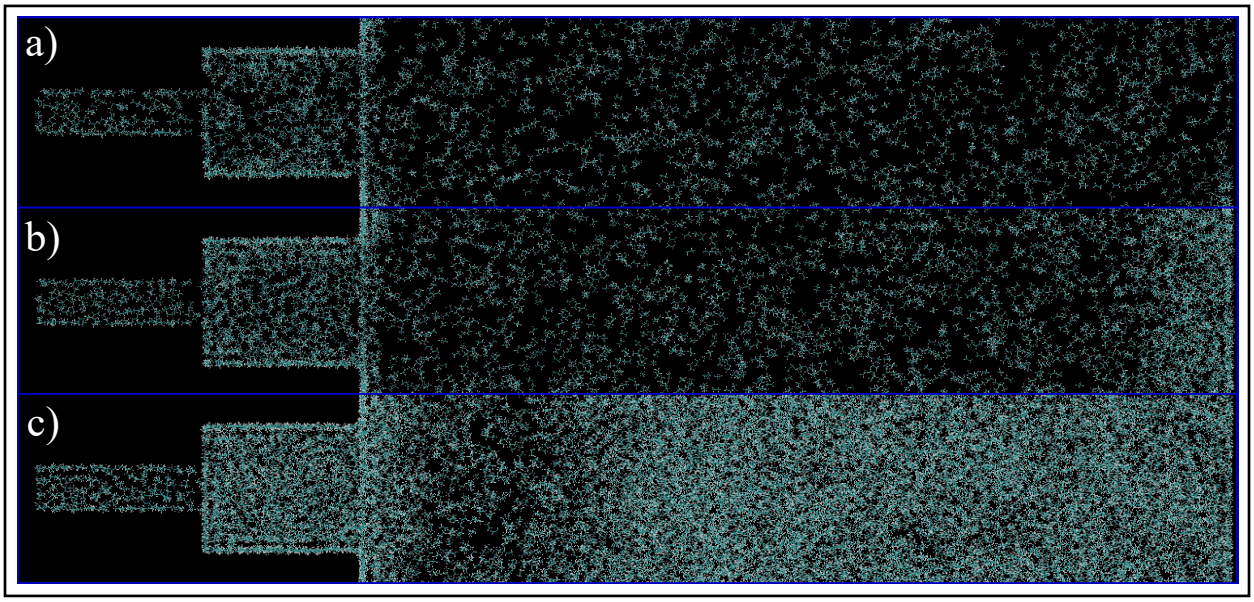


**Figure 2.14:** End of run images of the connected pore and bulk phase box, in gas (a), two phases (b) and liquid (c) conditions simulations. Cyan and white colors represent carbon and hydrogen atoms respectively.

In order to have an initial idea of phase and molecules behavior, the images of the system after 5 ns of simulation were investigated visually, which are shown in **Figure 2.14**, and **Figure 2.15**. For Case 1 (gas phase – a, d, g) and Case 3 (liquid phase – c, f, i), the fluid molecules behave similarly as the singles pore simulation, where there is a layer of high concentration of molecules near the walls of the 5 nm pore with a predominance of heptane molecules, and dispersed and agglomerated molecules in the middle of the pore, for Case 1 and Case 3 respectively. However, for Case 2 (2 phases – b, e, h) even though it had the same behavior for molecules near the wall as the single pore simulation, the middle of the pore constitutes of a dispersed phase of molecules, with a high concentration of ethane in contrast to a high concentration zone, rich in heptane. This observation can signify that when in contact to a smaller pore, the heptane and part of the molecules of the molecules tend to migrate to the 2 nm pore.

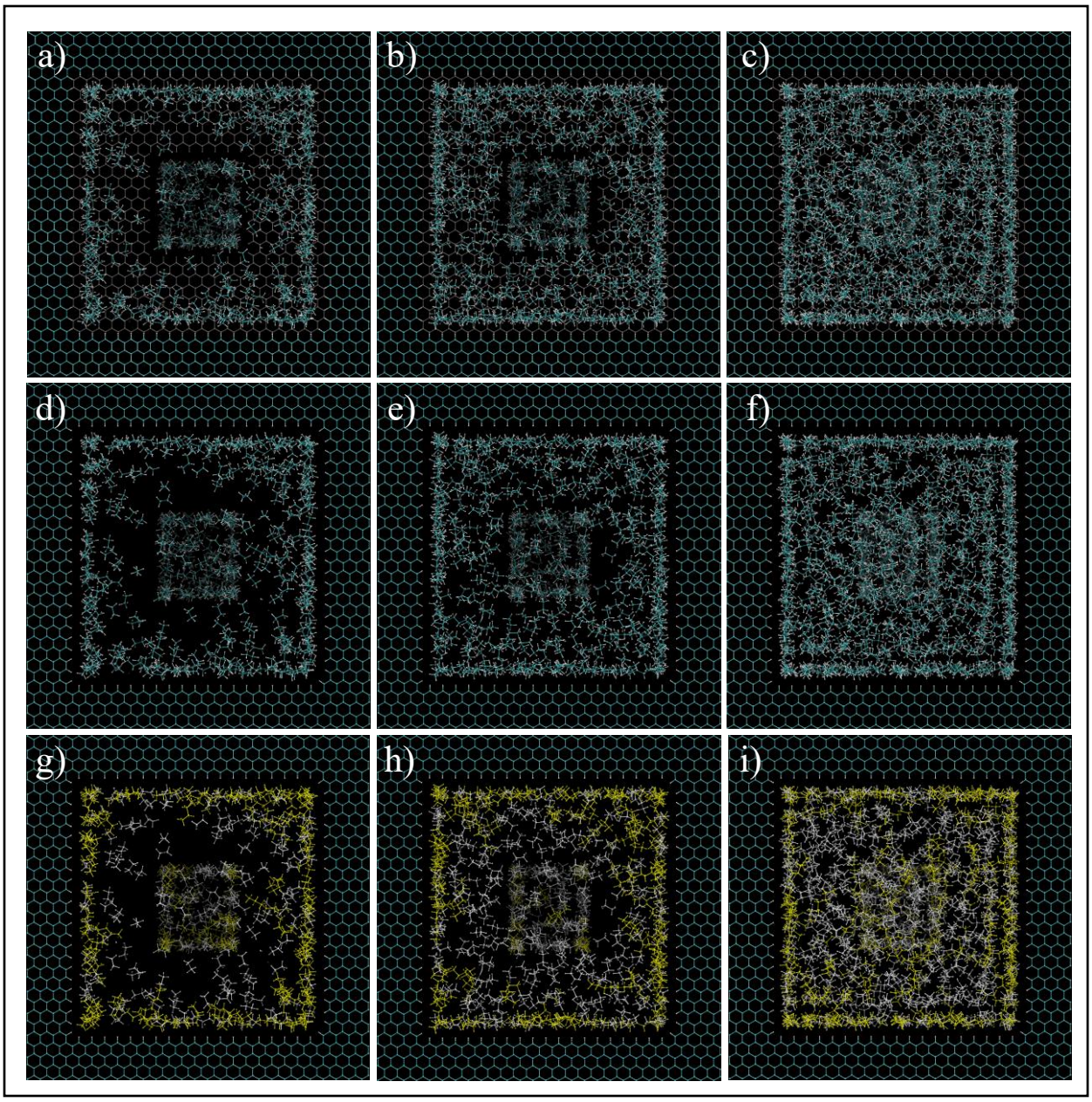


**Figure 2.15:** Ethane/Heptane mixture simulation in two connected nanopores at a), d), and g) Case 1, b), e) and h) Case 2, and c), f) and i) Case 3. Images d), e), and f) are the same as a), b), and c), but the 2 nm pore wall entrance is not shown in the formers. Cyan and white spheres, for images at first and second rows, are carbon and hydrogen atoms respectively. Yellow and white colors are heptane and ethane molecules respectively, for images at third row.

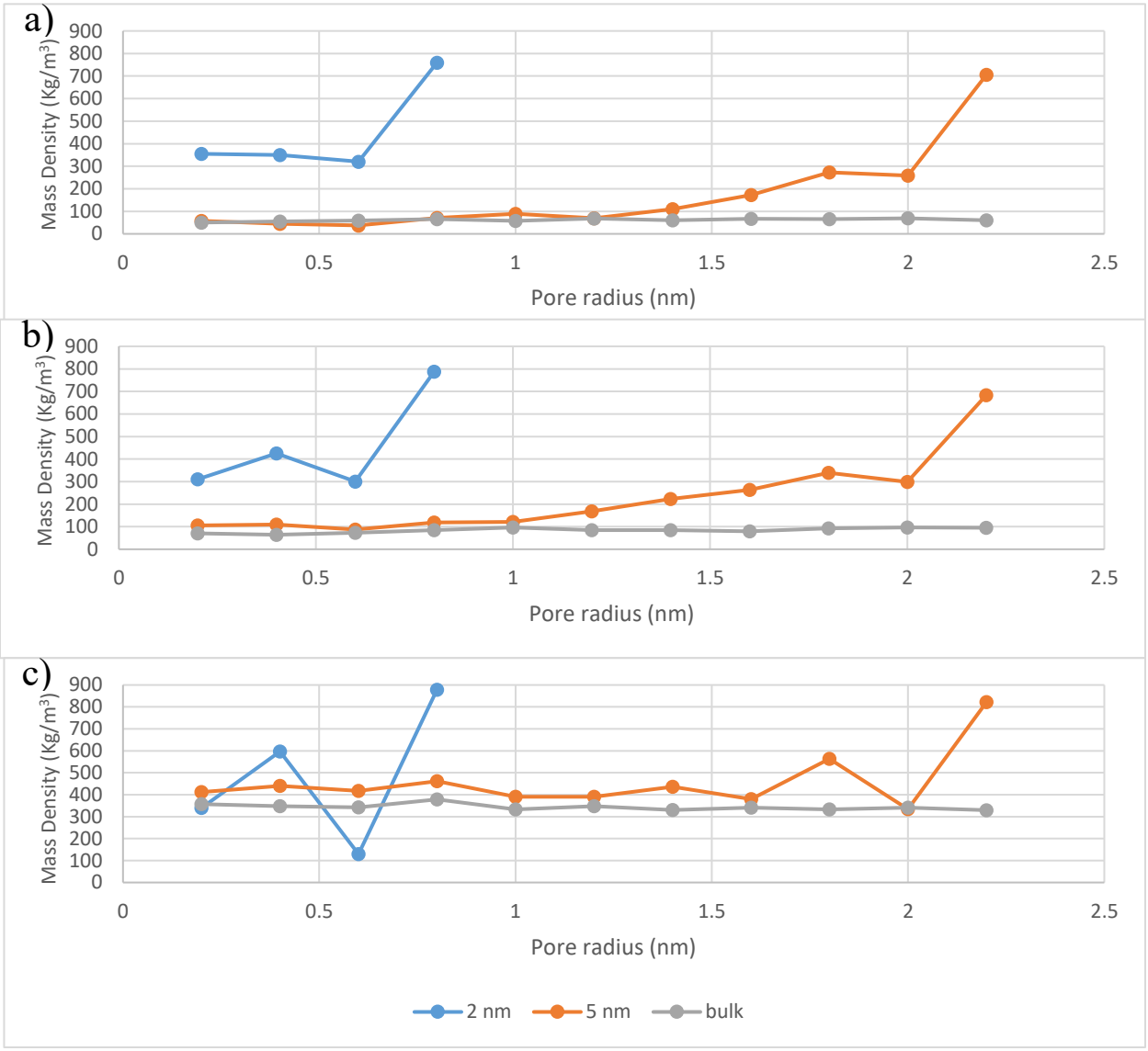


**Figure 2.16:** Mass density variation over pore radius for Case 1 (a), Case 2 (b) and Case 3 (c).

A quantitatively analysis was also performed to further investigate our previous visual observations. Firstly, the mass density over the pore radius was analyzed and the output can be found in **Figure 2.16**. For all cases, a similar trend line for both pores are observed, where there is a peak in density at the closest radius to the pore walls, which can mean an adsorption phenomena. In addition, both pores give a second peak, right after a depression in density, moving away from the pore walls, which can be interpreted as a second layer of adsorption. However, the mass density for both peaks are higher in the 2 nm pore compared to the 5 nm one. In addition, the

density observed at the center of the gas, and 2 phase condition, is close to the liquid condition density. It can be concluded that the effect of nanoconfinement in mass density increases with the pore size reduction.

### 2.3.3.2. Composition Alteration

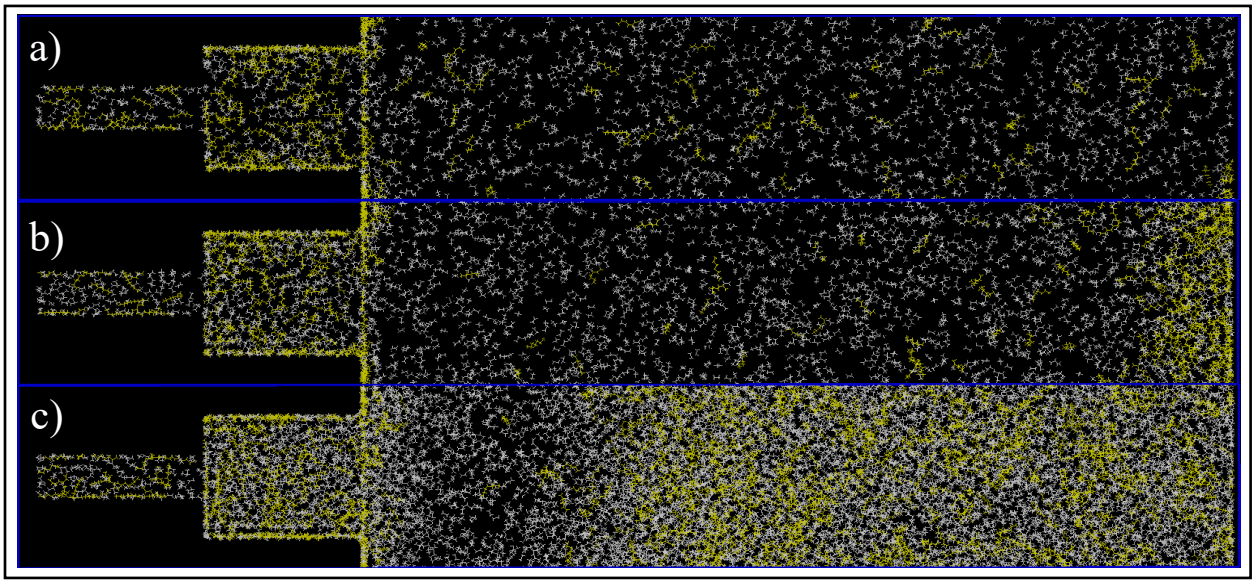


**Figure 2.17:** End of run images of the connected pore and bulk phase box, in gas (a), two phases (b) and liquid (c) conditions simulations for composition alteration analysis. Yellow and white colors represent heptane and ethane molecules respectively.

Similarly to the single 5 nm pore, the composition alteration of the 30/70 wt% ethane/heptane mixture was studied. Firstly, images at the end of simulation were investigated for a qualitatively analysis and they are shown in **Figure 2.17**. It is visible for all cases that there is a higher concentration of yellow color, which represents heptane molecules, inside the pores in detriment to its concentration in the bulk phase, where there is a predominance of white color, ethane molecules. In addition, for Case 2 and Case 3, **Figure 2.17b** and **Figure 2.17c** respectively,

it is possible to notice that the heptane molecules that were closer to the pores were the ones to firstly migrate inside of it, and in consequence it generates a rich ethane area of ethane at area adjacent to the entrance of the pore. Further, if compared to the gas simulation, **Figure 2.17a**, the molecules in this area are similarly dispersed with a void space in between, black color in figure, and they move more freely, which represent characteristic of a gas phase. Even though this is more visible and justifiable for Case 2, two phase gas and liquid, it also seen for fewer areas in Case 3. This observation foment the idea that nano-confinement can lead to phase transition, in addition to compositional alteration, not only inside the pores, but also at its entrance.

**Table 2.2:** Initial and final heptane mass fraction in 2 nm, 5nm, pores and bulk mediums**.**

| Domain | Initial (i) | Case 1 (f) | Case 2 (f) | Case 3 (f) |
|---|---|---|---|---|
| 2 nm Pore | 0.11 | 0.2188 | 0.1352 | 0.137 |
| 5 nm Pore | 0.11 | 0.1488 | 0.1322 | 0.118 |
| Bulk | 0.11 | 0.0757 | 0.047 | 0.1039 |

A qualitatively analysis was important to visualize the molecules pattern and concentrations, but it is difficult to examine the contrast between the 5 nm to the 2 nm pore. When the pictures were taken, a lateral view of the pore was shown, and since the cross section area of the 5 nm pore is higher than the 2 nm pore, it apparently appears that the concentration of heptane is higher in the 5 nm pore, which may not be the case. For this reason a quantitatively analysis is necessary. Firstly, the overall heptane mole fraction inside the pores and in bulk phase were

computed and are shown in **Table 2.2**. As expected, the overall heptane mole fraction was higher inside the pores, when compared to bulk medium, in all cases. Further, this parameter was even higher in the 2 nm pores compared to the 5 nm pore in all cases. This observation is in concordance to the increase in mass density of the pores, which reinforce the idea that nano-confinement effect in compositional alteration increases with the decrease of pore size.

### 2.3.4. Water and Hydrocarbons Fluids

In this section, water is introduced as a second immiscible fluid to the hydrocarbon mixture. This setup is used to simulate the preexisting water in the shale nano-pores prior to hydrocarbon accumulation, and examine the possibility of oil and gas displacement in the nanopore through water injection. The objectives include analyzing the effect of different wettability scenarios on adsorption and concentration of hydrocarbon molecules in the nanopore, while the phase behavior of hydrocarbon mixture is monitored.

#### 2.3.4.1 Surface Affinity Alteration

The wettability behavior of reservoir pores can possibly influence the adsorption and desorption of fluids. In order to observe this phenomena in association to nanoconfinement, two different surfaces were generated.

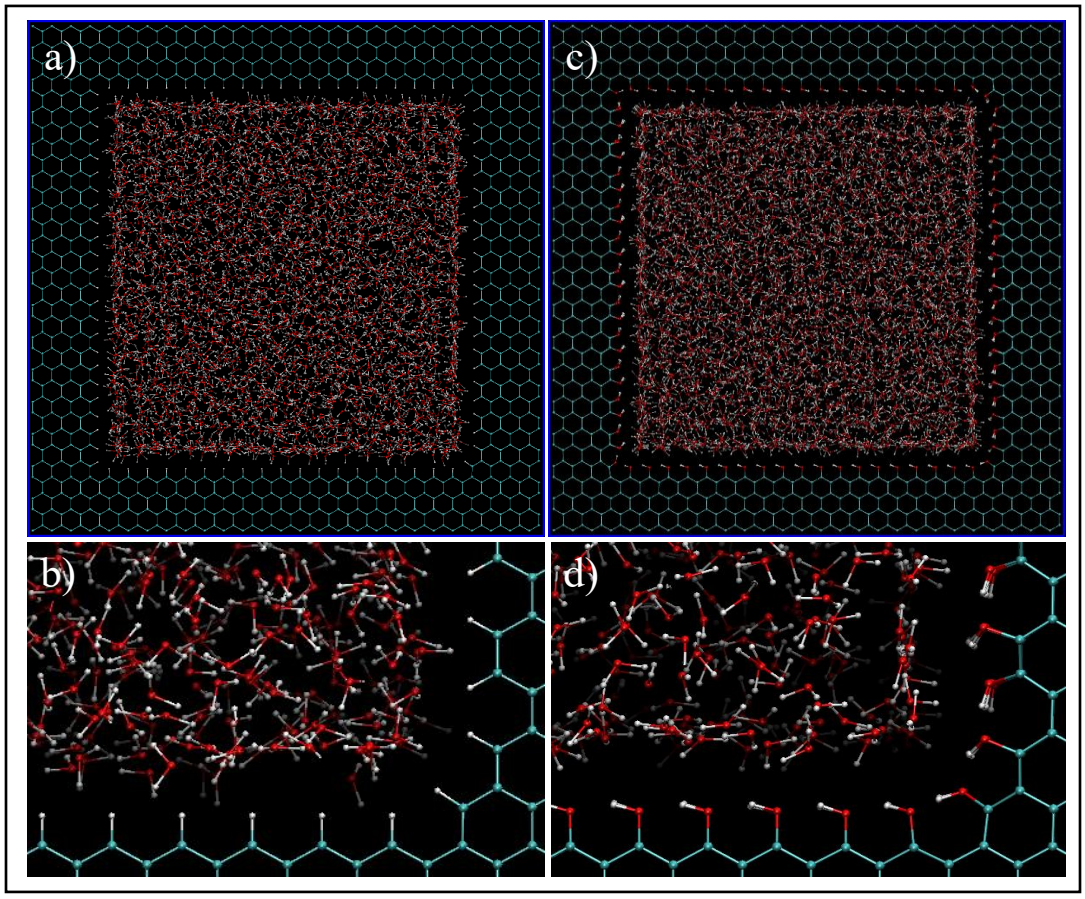


**Figure 2.18:** Configuration of H-Surface (a, c) and OH-surface (b, d) in presence of water. Cyan, white, and red spheres are carbon, hydrogen, and oxygen atoms respectively.

For H-Surface, also called here oil-wet surface (ow), **Figure 2.18a** and **2.18d**, Hydrogen (-H) was inserted to the dangling bonds of the carbon atoms on the surface, consequently creating a covalent bond between them. This type of bond does not create fluctuations on the electron density, therefore no poles are generated. It is expected that H-Surface would generate characteristics of a non-polar molecule, and thus attract similar molecule such as hydrocarbons, which gives it an oil-wet behavior. For OH-Surface, also called here water-wet surface (ww), **Figure 2.18b** and **2.18d**), a Hydroxyl group (-OH) was added instead of only Hydrogen, which creates an ionic bond with the carbons on the surface because of the high difference in partial charges of involved atoms. The ionic bond does disturb the electron density, which generates poles trough the surface. The

expected result is that OH-Surface exhibits a polar molecule characteristic, which can also form Hydrogen bonds since O is present, and thus attract similar polar molecules such as water (water-wet behavior). In this section, we investigated the ability of the proposed shale graphite pore to give oil-wet and water-wet characteristics upon adding H and OH atoms/bonds on the surface.

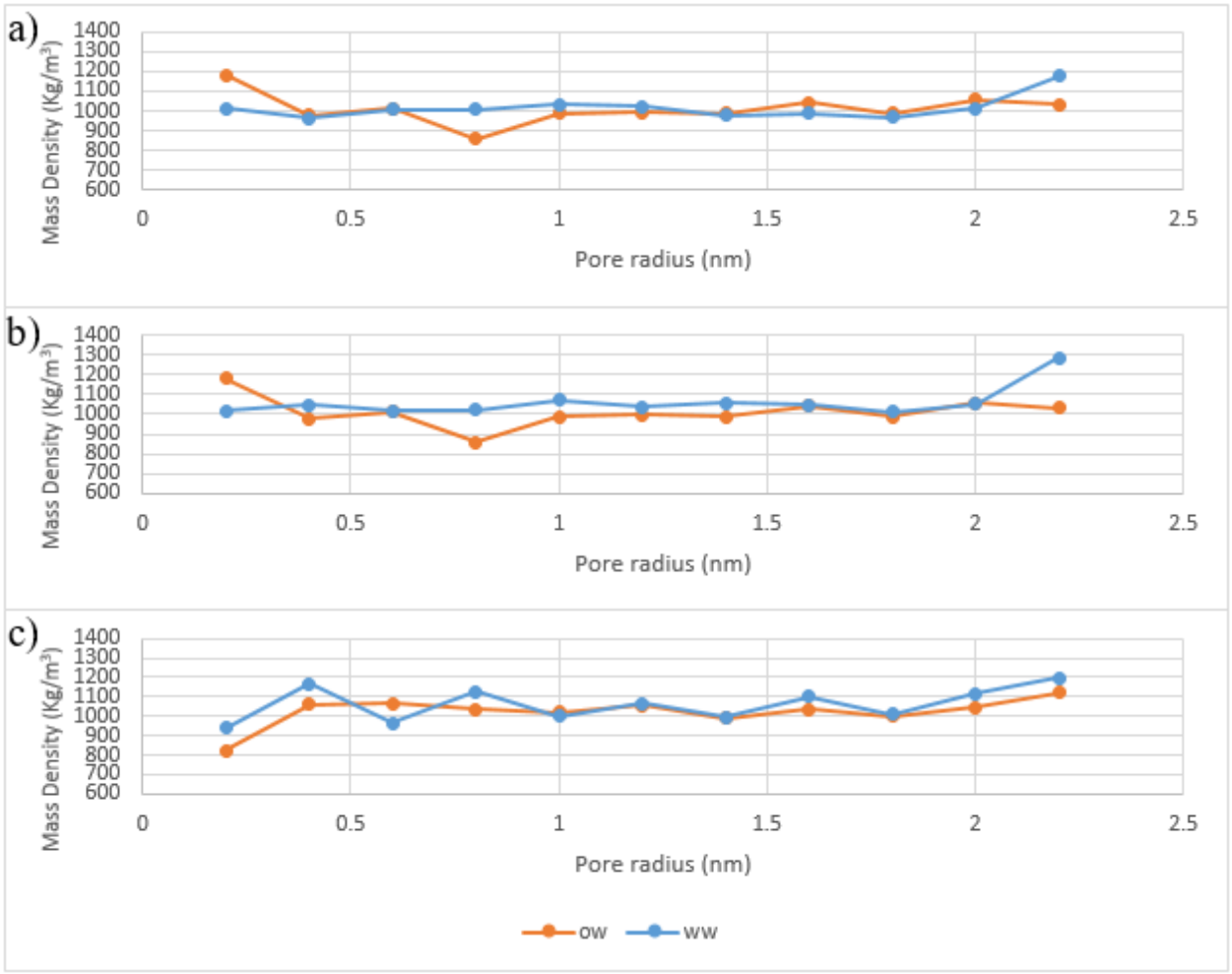


**Figure 2.19:** Water mass density variation over pore radius for Case 1 (a), Case 2 (b) and Case 3 (c).

To study the adsorption behavior, the surfaces were firstly subjected to only water. Three simulation setups were considered with the same ethane/heptane mixture temperature and pressure conditions that would give gas (Case 1), two-phase liquid/gas (Case 2), and liquid (Case 3). The

mass density of water was monitored radially, and the results are shown in **Figure 2.19**. Although the density remains fairly constant inside the pore, near the pore walls, a trend of density increase is observed for the water-wet pore, while the density remains constant or decreases near the pore surface for the oil-wet pore. This behavior can be explained by the interaction forces between water and the surfaces. The water-wet pore has hydrogen bonding with water, which is much stronger than the van der Waals interactions that the oil-wet pore can have. Consequently, the water-wet pore attracts the water molecules, creating a layer of adsorbed molecules, which then increases the mass density over the surface. This adsorption layer on the oil-wet pore can be seen in **Figure 2.18d**, where the water molecules are in an 'organized' structure, compared to dispersed molecules near the oil-wet surface (see **Figure 2.18b**).

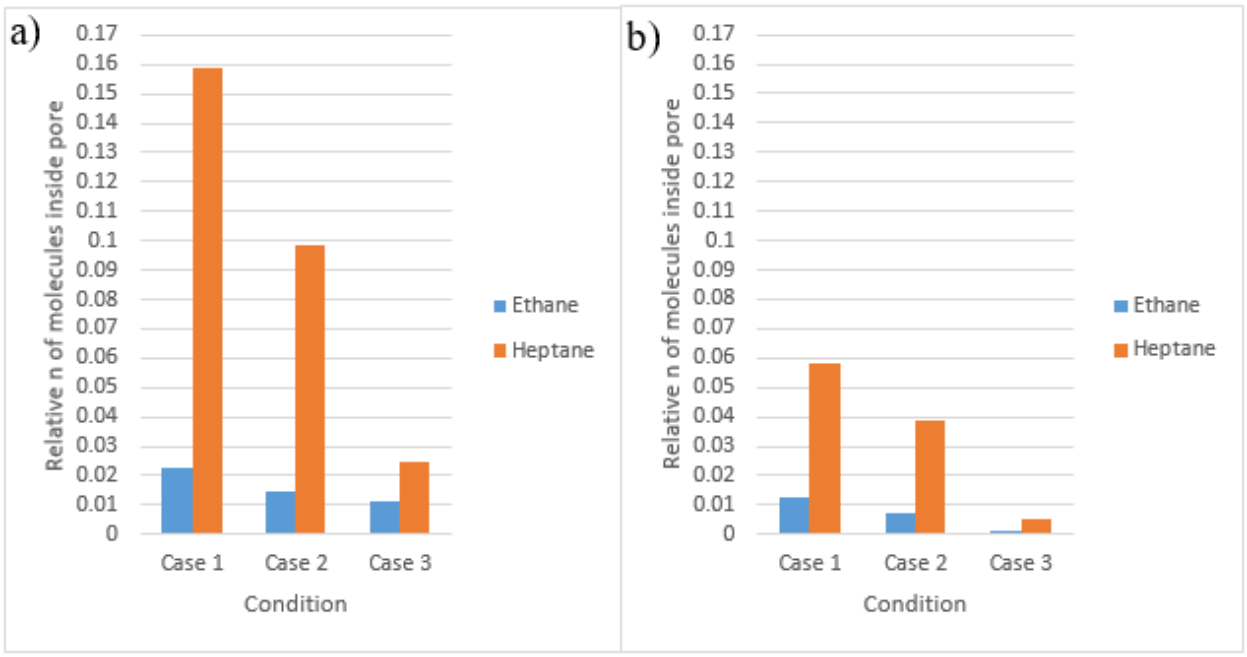


**Figure 2.20:** Relative number of molecules that entered a) oil-wet, and b) water-wet pores.

Next, mixture of 30/70 wt% ethane/heptane mixture was introduced to the system as a bulk phase outside the pore containing the pre-adsorbed water molecules. In order to investigate the

effect of pore wetting behavior on the transport of hydrocarbon molecules for different phases, a total of six simulations were performed. Note that all the simulations were performed for 5 nanoseconds. Since ethane contributes to the majority of the system mass, and consequently in number of molecules, number of ethane and heptane molecules were divided by the total number of molecules in the system, which gives a relative number of molecules. This dimensionless number could be used to compare the preferential adsorption of hydrocarbon molecules. The results are shown in **Figure 2.20**. We can understand from the results that at all conditions, the relative number of hydrocarbon molecules were higher in the oil-wet pore, which confirms the wettability behavior of the pore since both pore molecules and hydrocarbon have a nonpolar characteristic. Secondly, the relative number of molecules decreases from Case 1 to Case 3. Since molecules in gas phase have less restriction to move, the molecules are dispersed, and they can come in contact to the pore more often and interact with the surface. In addition, the higher temperature of the system, and the consequent higher molecule's velocity, also facilitates the movement of the gas molecules. If this interaction is higher than the pre-adsorbed water molecules interaction with the pore walls, these hydrocarbon molecules would then replace water molecules. Thirdly, the relative number of heptane molecules that entered the pore is higher for all conditions and pores. This observation confirms the idea that the shale pore preferentially adsorbs heptane over ethane as mentioned in the previous sections.

#### 2.3.4.2 Spontaneous Imbibition and Drainage

These two similar yet opposite processes are important to observe the wettability of the pore, but also the displacement mechanism in which hydrocarbons are extracted from pores. Imbibition is the process where the wetting phase displaces the non-wetting phase and drainage is the exactly opposite. In this section, the oil-wet and water-wet 5 nm nanopores were firstly subjected to a only hydrocarbon medium at Case 1 conditions, gas phase (260 °F, 300 psi), in order to simulate the migration, accumulation, and adsorption events in a reservoir. Then, the molecules outside and on the left side of the pore were removed and replaced by a water. This water box was previously simulated at the same temperature and pressure conditions in order to be equilibrated. Through introduction of the water box, we expected to simulate a drainage process for the oil-wet pore, and an imbibition process for the water-wet pore. However, here no pushing force or pressure was applied to the left side of the water box to force it to go thought the pore, so the only driving force that would make the water molecules enter the pore would be the molecular interactions between them and the pores. Then, with these parameters, we expected to simulate a spontaneous drainage/imbibition rather than forced ones. One issue for simulating a spontaneous process is that the simulations takes longer to complete, and probably the water will not enter the oil-wet pore for a drainage process. For this reason, the simulations were performed for 15 ns (relatively a long

time for MD simulations), but the processes do not seem to be completed. The longer simulation time limited us to choose only Case 1 (hydrocarbon mixture in gas phase) for this study.

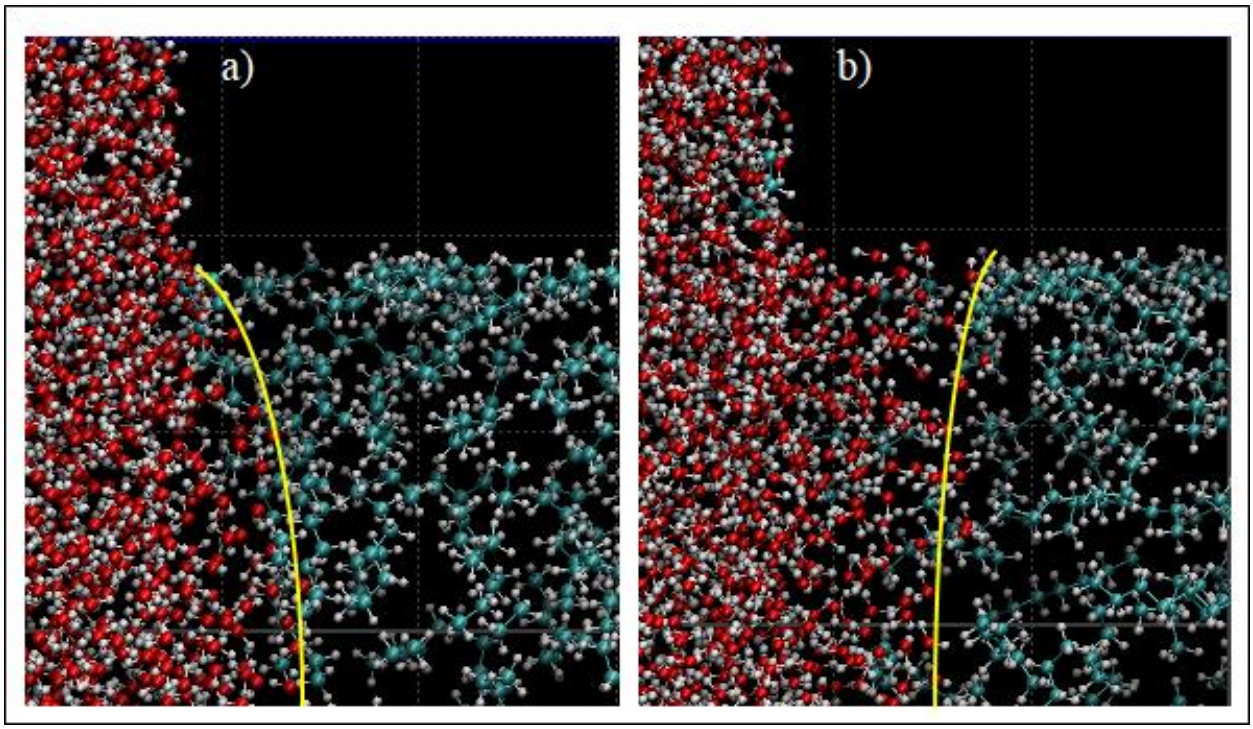


**Figure 2.21**: Picture of the half-pore entrance after 15 nm of simulation of a) drainage, and b) imbibition process. The yellow line represents the apparent shape of the water phase meniscus. Red, cyan and white colors represent oxygen, carbon, and hydrogen molecules respectively.

Similar to previous sections, the simulations results were analyzed both qualitatively and quantitatively. For the qualitative analysis, firstly the motion of the water molecules were tracked every 0.01 ns in order to observe the displacement mechanism of hydrocarbon molecules by water molecules. For the drainage process, water molecules required more time to enter the oil-wet pore, and to do so, they firstly displaced the oil molecules at the center of the pore. Then, as the interface meniscus progressed, the water molecules displaced the molecules adjacent to the pore surface to the center of the pore. It is important to highlight that no oil molecules were desorbed from the

surface of the pore. The water molecules entered the pore much faster for the imbibition process. In addition the mechanism was opposite to the drainage, in where the water molecules firstly interacted with the pore surface, by a strong hydrogen-bonding interaction, which caused desorption of oil molecules and their displacement. As the water molecules advanced toward the walls, they got slower until they reached the meniscus, then the water phase moved toward the pore as a continuous phase. At the end of the simulations, these opposite mechanisms resulted in contrasting meniscus shapes, which can be seen in **Figure 2.21**. Note that our observations are aligned with what we expected regarding the contact angle of the oil/water interface for oil-wet and water-wet surfaces. Here, the contact angle of both drainage and imbibition process could be measured from the apparent shape of the meniscus close to the wall. However, we decided to not present exact numbers for contact angle since we suspected the processes were not completed. Nevertheless, we can definitely observe if the angles were lower or higher than 90°. For the drainage setup, **Figure 2.21a,** the contact angle is higher than 90°, which implies that water is the non-wetting fluid, and that the process of water entering the pore is a drainage. In the imbibition setup, **Figure 2.21b,** the contact angle is lower than 90°, which implies that water is the wetting fluid, and that the process of water entering the pore is an imbibition.

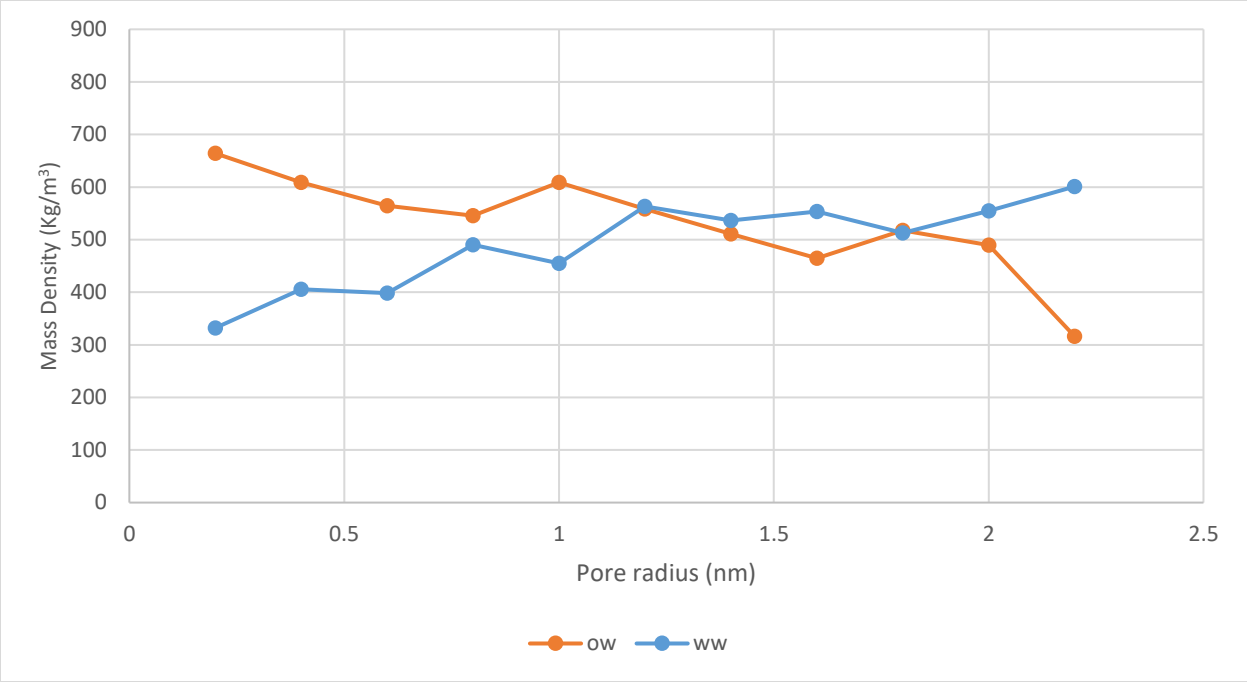


**Figure 2.22:** Water meniscus mass density variation over pore radius for Case 1 in oil-wet and water-wet pores.

For the quantitative analysis, the number of water molecules that went inside the pores and the mass density of the water meniscus were measured. The number of water molecules that entered the water-wet pore, 263, was much higher than the oil-wet pore, 126. This number reflects how easily the water molecules could enter the pore, and it confirms that the hydroxyls on the surface of the water-wet pore gave it a water-wet behavior, and thus it prefers to adsorb water. Furthermore, the mass density of the meniscus was monitored through the pore radius and it is shown in **Figure 2.22**. The shape of the curves reflects the apparent shape of the meniscus itself, shown on **Figure 2.21**. We can observe that for the oil-wet pore during the drainage process, the curve has a peak at the center of the pore, and then it is followed by a descendant curve until it reaches its minimum at the pore walls. The water-wet pore has an opposite trend, as at the center of the pore the mass density is the lowest, and it reaches its maximum at the surface. These observations confirm that adding –H or –OH to the dangling bonds on the surface can define the

wettability of the pore to be oil-wet or water-wet respectively without changing the molecular type of the rock. Furthermore, in this sections we could perform and analyze a drainage and imbibition process with the oil-wet and water-pore pore models respectively.

#### 2.3.4.3. Water Injection

Water injection is a common recovery technique used in petroleum reservoirs. As the name suggests, this method consists of pumping water trough injection wells nearby the production well, from that the oil is extracted. This approach is usually used when the natural pressure of the reservoir is not sufficient, or has decreased to uneconomical levels, so a secondary recovery technique has to be implemented to make the well economically viable. In order to simulate this process through MD simulations, we implemented a piston system to the models used in previous simulations where a box of water was introduced at the entrance of the pore. The pistons consist of two graphene walls, but its interaction parameters were set to zero in order to not interfere with the process, consequently its only effect was to push the water inside the pore. Two set of pistons were introduced to the system, one on the left side of the simulation box, and one on the right side. The right piston did not move throughout the simulation, while an external force was added to the left piston, so it could apply pressure to the water box. The system can be seen in **Figure 2.23.** In this section, the fluids were subjected to Case 1 and Case 3 conditions, gas and liquid phase respectively, and H-Surface and OH-Surface were used to study the effect of wettability, and therefore, a total of four simulations were performed. The objectives of these simulations were to observe water injections in nanopores and study the effect of nano-confinement, surface affinity, and fluid phase type on the displacement mechanism and recovery factor for unconventional shale reservoirs.

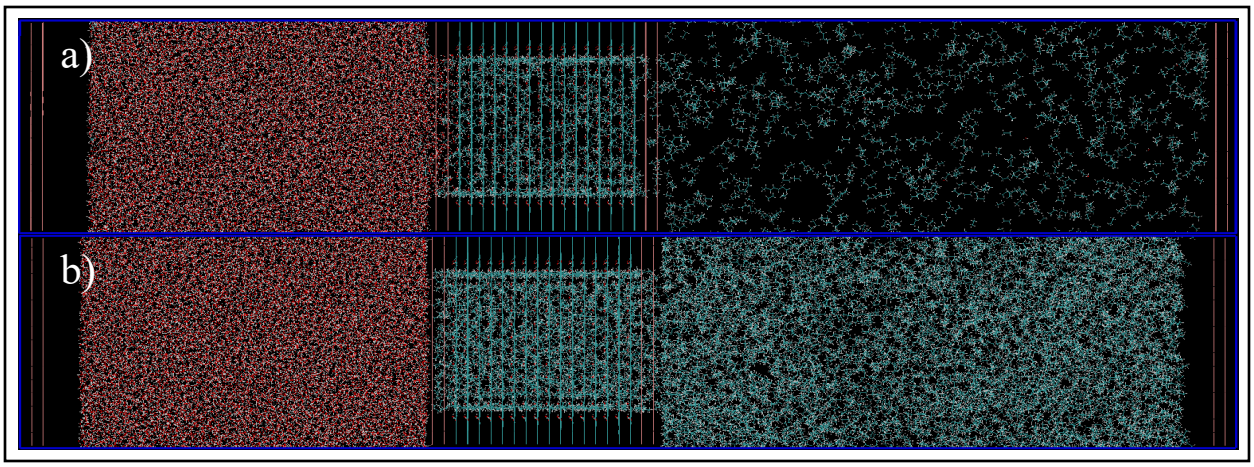


**Figure 2.23:** Water injection models with pistons at the left and right sides of the simulation box for the OH-Surface for a) Case 1, and b) Case 3. Cyan, white and red spheres represent carbon, hydrogen, and oxygen atoms respectively.

The displacement mechanism was observed and analyzes through the imaging the movement of molecules at different time steps and it is shown in **Figure 2.24**. In this figure, only Case 3 (hydrocarbon liquid phase), is shown since the mechanism was similar for both cases. Prior to water injection, a layer of adsorbed oil molecules is observed on both surfaces. When water is injected, it seems that this layer resists to the flow of water molecules nearby the pore walls, and this resistance is even greater at the pore corners since there is a higher accumulation of hydrocarbon molecules in this area. Since the water molecules experience a lower resistance to movement at the center of the pore, they first displace the hydrocarbon molecules in this area. As the injection proceeds, the hydrocarbon molecules at the center of the pore are subsequently displaced. At the pores walls, the difference between the radicals added to the dangling bonds on the surface (–H and –OH bonds), starts to affect the flow regime. It is harder to desorb the oil molecules at the H-Surface, compared to the OH-Surface, since the interaction between the atoms on the surface is higher between hydrocarbon molecules than for water molecules, which causes a

higher resistance to flow of water molecules. Consequently, the water front observed for the OH-Surface is always ahead of that for the H-Surface at the same time step.

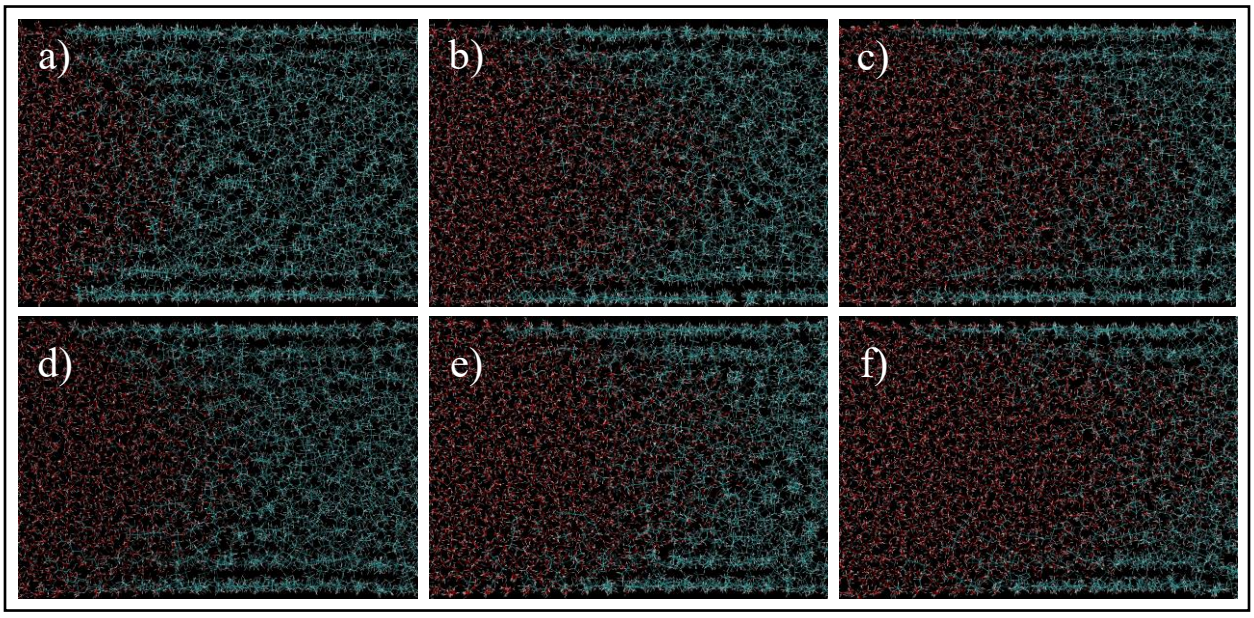


**Figure 2.24:** Water meniscus inside the pores at Case 3 and a), b), and c) represents H-Surface, and d), e), f) represents OH-Surface. Pictures were taken from frames 1nm apart. Cyan, white and red spheres represent carbon, hydrogen and oxygen atoms respectively.

At the end of the injection, when the pistons reached the pore entrance, picture of the pores exit where taken and are shown in **Figure 2.25.** Firstly, we compare the effect of hydrocarbon phase, liquid versus gas. From **Figure 2.25**, it is observed that hydrocarbon molecules were displaced to a greater extent for Case 1 (gas) compared to Case 3 (liquid). This observation can be explained by the fact that the hydrocarbon molecules for Case 1 (gas phase) are subjected to a higher temperature and consequently have more freedom to move. The higher temperature of Case 1 causes the molecules to have a higher velocity and vibration, which weakens the interaction between the hydrocarbon molecules and the pore walls, compared to the lower temperature for Case 3. When the surfaces are compared, more hydrocarbon molecules remained absorbed on the

H-Surface when compared to the OH-Surface. This behavior was expected and again can be explained by the higher interaction forces between the –H radical on the surfaces and the oil molecules. It was interesting to observe a layer of adsorbed oil molecules on the pore walls and its pattern, where it mostly accumulated at the corners, even after the injection of pressurized water molecules.

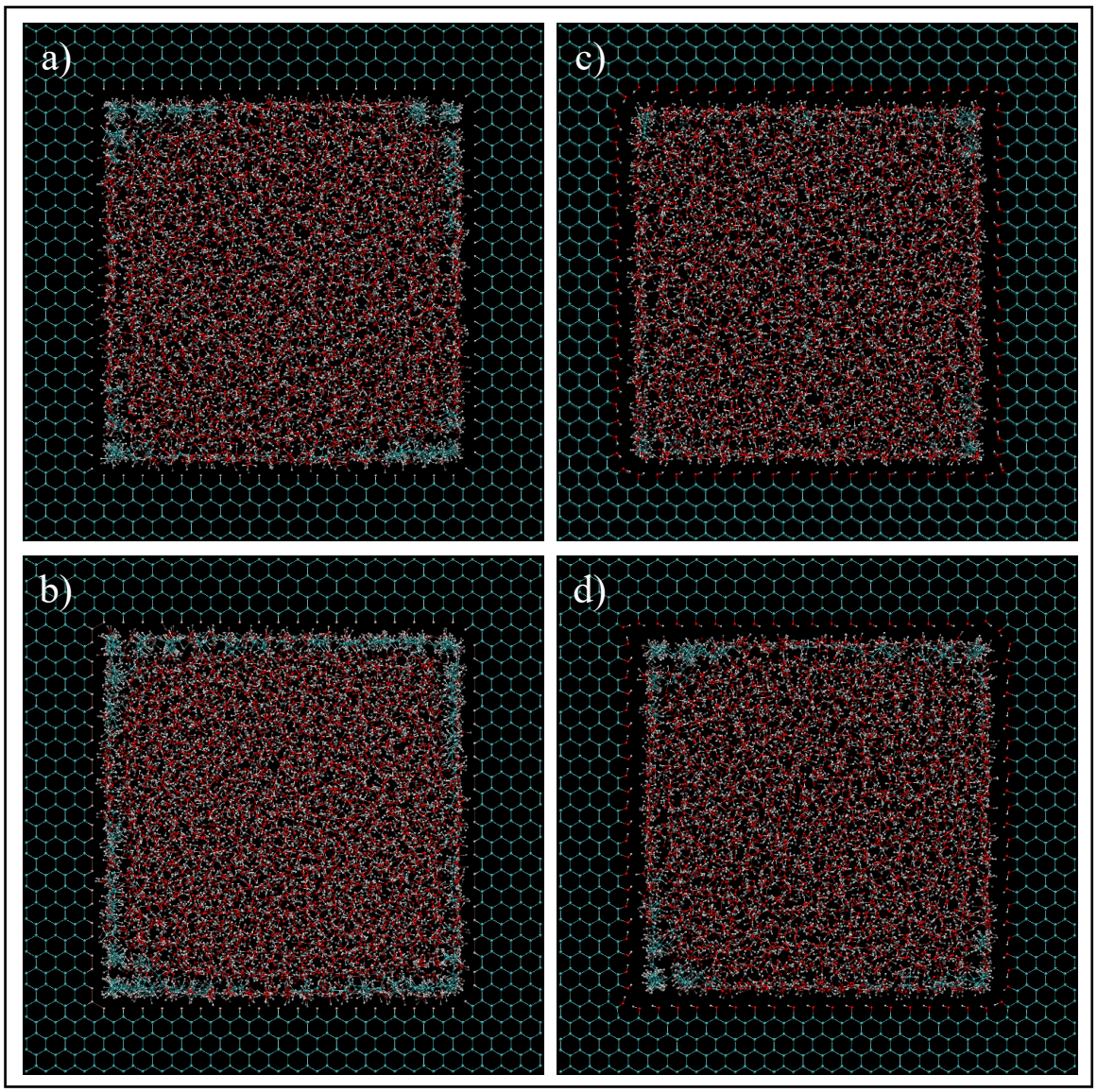


**Figure 2.25:** Pictures at the exit of the pore after water injection. First row is for Case 1 (gas) and second row for Case 3 (liquid), and a) and b) for H-Surface and c), and d) for OH-Surface. Cyan, white and red spheres represent carbon, hydrogen and oxygen atoms respectively.

Lastly, recovery factor of hydrocarbon molecules was acquired. This number was calculated by dividing the difference of the number of molecules that remained inside the pore after water injection and the initial number of hydrocarbon molecules inside the pore prior to water injection, by the initial number of hydrocarbon molecules in the pore. The results can be seen in **Table 3**. From this table it can be understood that alteration of surface radicals, which changes the pore wettability, is the most influential factor. When hydrocarbon is in liquid phase (Case 3), pore wettability results in 10% difference in recovery. Although, we do not believe that these values can be yet extended to macroscale simulation models without further analyses of the molecular scale system, these results can be used to compare the efficiency of $CO_2$ or $N_2$ injection EOR/EGR (enhanced oil/gas recovery).

**Table 2.3:** Recovery factors for Case 1 and 3 and H-Surface and OH-Surface.

| | Recovery (%) |
|---|---|
| Case 1 (gas) - H | 81.68 |
| Case 3 (liquid) - H | 78.58 |
| Case 1 (gas) - OH | 87.69 |
| Case 3 (liquid) - OH | 89.57 |

# 3. Conclusions

In this chapter, a summary and conclusions of the study discussed in this document, along with suggestions for future work, are presented.

## 3.1. Summary and Conclusions

In this study, the nanoconfinement effect on hydrocarbon fluid phase behavior and composition in a fully atomistic shale pore was analyzed during multiple processes. Firstly, a literature review on molecular dynamics simulation of rock-fluid interactions in geological resources was performed in order to acquire sufficient knowledge to identify problems and in what manner the models could be improved, which was presented in Chapter 1. Next, an improved pore model is proposed and used to investigate the nanoconfinement effect on the phase and compositional behavior of binary mixture of two hydrocarbon molecules in organic shale rocks in Chapter 2.

Multiple research studies have been critically reviewed in Chapter 1, but it is important to highlight the more realistic models. To represent the pore minerals, a fully atomistic model, where all the atoms have individual parameters is preferred over Leonard-Jones sphere. Inorganic matter in shale pores are usually represented by calcite, quartz, or mica while organic matter is modeled as graphite or kerogen. Block carving is the more realistic technique to fully account for the pore walls nanoconfinement effect. A hydrocarbon mixture, instead of a single component fluid, can better represent the oil encountered in shale. Alteration of radicals, –H or –OH, for more oil-wet and water-wet respectively, to the dangling bonds for block carving technique proved to be an important tool to alter surface affinity. Density and interaction energy are one of the most important

parameters used to analyze fluid adsorption, composition, as well as contact angle measurements in MD simulations of geological resources. Although the phase transition of oil mixture, adsorption mechanisms, surface wettability manipulation, and oil displacement has been studied before, these models either used simplistic pore crystal structure and geometry or considered single component hydrocarbon fluids. More ever, neither of the previous studies considered a network of confined spaces with different sizes, to represent the distribution of pore sizes of the heterogeneous porous rock.

In Chapter 2, a fully atomistic squared graphite pore that satisfies all the requirements of the force field in use is proposed. This pore uses a complicated and more realistic geometry that accounts for the total effect of wall surfaces, and vertices effects. The pore is then used to extensively study the phase behavior of hydrocarbon molecules and water under nanoconfinement effect while the nanopores can communicate with the bulk. In addition, for the first time, the effect of pore aperture size on hydrocarbon fluid phase behavior and composition was studied in a single simulation by two smoothly connected nanopores (5 and 2 nm) which communicated with the bulk as well. This model can more realistically represent the pore size heterogeneity encountered in shale nanopores.

The simulations could successfully replicate gas, two phases, and liquid phase characteristic in bulk. Nanoconfinement effect was proved to influence the mass density and composition inside the graphite pore. This density can be observed as a layer of adsorption of hydrocarbon molecules to pore walls, and a subsequent second layer of adsorption was also encountered in the majority of pore simulations. A higher concentration of hydrocarbons was observed at the squared pore corners and vertices. The graphite pore preferentially adsorbs heptane over ethane since the former has a longer carbon chain and consequently higher van der Walls

interactions with the nonpolar surface, thus changing the composition inside the pore. Gas and mainly two phase conditions were the most affected phases by nanoconfinement. It was found that, as expected, the smaller the pore cross sectional area, the higher the influence of nanoconfinement on mass density and fluid composition. The manipulation of radicals on the surface, –H or –OH, was proved to alter the surface affinity to represent a more oil-wet and water-wet characteristics respectively. When a water box is introduced at the entrance of the pores after hydrocarbon accumulation, it forms a meniscus with a higher and lower than 90° for the H-Surface and OH-Surface respectively. When pressure is exerted by pistons on the water box, water molecules encounters less resistance and displaces the oil molecules more easily in the OH-Surface compared to the H-Surface. The recovery factor for the OH-Surface was 10% higher than that of the H-Surface for Case 3 (liquid hydrocarbon phase). After water injection, the H-Surface resulted in a more prominent oil layer compared to the OH-Surface, and this layer was thicker for Case 3 (liquid hydrocarbon phase). Higher hydrocarbon accumulation was observed at the vertices. Finally, the increase in density, caused by the adsorption layer on the nanopore, proved to alter OIP since this value would be underestimated without the modified density. The recovery factor calculated here can be useful to compare different gas injection oil and gas enhanced recovery (EOR/EGR) techniques under nanoconfinement conditions.

### 3.2. Future Work

To expand the applicability of the model used and to better understand the phenomena observed here, some recommendations for future work can be given. The pore model can be substituted by quartz or calcite, in order to study adsorption behavior by the inorganic matter that is also a constituting part of shale rocks. A concept of mixed-wet pore can be produced, in where the dangling bond would be connected to a distribution of (-H) and (-OH) radicals. A more complicated oil mixture, involving polar and nonpolar molecules, and longer chain hydrocarbons, can be applied to observe distinct adsorption and phase behavior of such systems. A correlation can be created from the oil adsorption layer to improve OIP calculations. A comparison of recovery techniques, such as water, $CO_2$, and $N_2$ can be performed at the two-connected nanopores, and the desorption mechanism can be studied to improve recovery methods and predictions of unconventional reservoirs recovery.

## References


(1) Tang, Dai, Yeong-Eun Yoo, and Daejoong Kim. "Molecular dynamics simulations on water permeation through hourglass-shaped nanopores with varying pore geometry." *Chemical Physics* 453 (2015): 13-19.

(2) Turgman-Cohen, Salomon, Juan C. Araque, Eric MV Hoek, and Fernando A. Escobedo. "Molecular dynamics of equilibrium and pressure-driven transport properties of water through LTA-type zeolites." *Langmuir* 29, no. 40 (2013): 12389-12399.

(3) Shirono, Katsuhiro, and Hirofumi Daiguji. "Molecular simulation of the phase behavior of water confined in silica nanopores." *The Journal of Physical Chemistry C* 111.22 (2007): 7938-7946.

(4) Yamashita, Kyohei, and Hirofumi Daiguji. "Molecular dynamics simulations of water uptake into a silica nanopore." *The Journal of Physical Chemistry C* 119.6 (2015): 3012-3023.

(5) Holmboe, Michael, and Ian C. Bourg. "Molecular dynamics simulations of water and sodium diffusion in smectite interlayer nanopores as a function of pore size and temperature." *The Journal of Physical Chemistry C* 118.2 (2013): 1001-1013.

(6) Liu, Bing, Chao Wang, Jun Zhang, Senbo Xiao, Zhiliang Zhang, Yue Shen, Baojiang Sun, and Jianying He. "Displacement mechanism of oil in shale inorganic nanopores by supercritical carbon dioxide from molecular dynamics simulations." *Energy & Fuels* 31, no. 1 (2017): 738-746.

(7) Wu, Tiantian, Qingzhong Xue, Xiaofang Li, Yehan Tao, Yakang Jin, Cuicui Ling, and Shuangfang Lu. "Extraction of kerogen from oil shale with supercritical carbon dioxide: Molecular dynamics simulations." *The Journal of Supercritical Fluids* 107 (2016): 499-506.

(8) Yuan, Quanzi, Xueyan Zhu, Kui Lin, and Ya-Pu Zhao. "Molecular dynamics simulations of the enhanced recovery of confined methane with carbon dioxide." *Physical Chemistry Chemical Physics* 17, no. 47 (2015): 31887-31893.

(9) Wu, HengAn, Jie Chen, and He Liu. "Molecular dynamics simulations about adsorption and displacement of methane in carbon nanochannels." *The Journal of Physical Chemistry C*119.24 (2015): 13652-13657.

(10) Fang, Chao, Fei Zhang, and Rui Qiao. "Invasion of gas into mica nanopores: a molecular dynamics study." *Journal of Physics: Condensed Matter* 30.22 (2018): 224001.

(11) Sedghi, Mohammad, Mohammad Piri, and Lamia Goual. "Atomistic molecular dynamics simulations of crude oil/brine displacement in calcite mesopores." Langmuir 32.14 (2016): 3375-3384.

(12) Sedghi, Mohammad, Mohammad Piri, and Lamia Goual. "Molecular dynamics of wetting layer formation and forced water invasion in angular nanopores with mixed wettability." *The Journal of chemical physics* 141.19 (2014): 194703.

(13) Liu, Bing, Chao Wang, Jun Zhang, Senbo Xiao, Zhiliang Zhang, Yue Shen, Baojiang Sun, and Jianying He. "Displacement mechanism of oil in shale inorganic nanopores by supercritical carbon dioxide from molecular dynamics simulations." *Energy & Fuels* 31, no. 1 (2017): 738-746.

(14) Wang, Sen, Farzam Javadpour, and Qihong Feng. "Molecular dynamics simulations of oil transport through inorganic nanopores in shale." *Fuel* 171 (2016): 74-86.

(15) Yan, Hui, and Shiling Yuan. "Molecular dynamics simulation of the oil detachment process within silica nanopores." *The Journal of Physical Chemistry C* 120.5 (2016): 2667-2674.

(16) Stukan, Mikhail R., Patrice Ligneul, and Edo S. Boek. "Molecular dynamics simulation of spontaneous imbibition in nanopores and recovery of asphaltenic crude oils using surfactants for EOR applications." *Oil & Gas Science and Technology–Revue d'IFP Energies nouvelles* 67.5 (2012): 737-742.

(17) Sen, Wang, Feng Qihong, Zha Ming, Lu Shuangfang, Qin Yong, Xia Tian, and Chi ZHANG. "Molecular dynamics simulation of liquid alkane occurrence state in pores and slits of shale organic matter." *Petroleum Exploration and Development* 42, no. 6 (2015): 844-851.

(18) Chen, Cong, Jiamin Wan, Weizhong Li, and Yongchen Song. "Water contact angles on quartz surfaces under supercritical CO2 sequestration conditions: Experimental and molecular dynamics simulation studies." *International Journal of Greenhouse Gas Control* 42 (2015): 655-665.

(19) McCaughan, Jack, Stefan Iglauer, and Fernando Bresme. "Molecular dynamics simulation of water/CO2-quartz interfacial properties: Application to subsurface gas injection." *Energy Procedia* 37 (2013): 5387-5402.

(20) Santos, Mirella S., Luís FM Franco, Marcelo Castier, and Ioannis G. Economou. "Molecular dynamics simulation of n-alkanes and CO2 confined by calcite nanopores." *Energy & Fuels* 32, no. 2 (2018): 1934-1941.

(21) Zhong, Jie, Pan Wang, Yang Zhang, Youguo Yan, Songqing Hu, and Jun Zhang. "Adsorption mechanism of oil components on water-wet mineral surface: A molecular dynamics simulation study." *Energy* 59 (2013): 295-300.

(22) Moncayo-Riascos, Ivan, Jennifer de León, and Bibian A. Hoyos. "Molecular dynamics methodology for the evaluation of the chemical alteration of wettability with organosilanes." *Energy & Fuels* 30.5 (2016): 3605-3614.

(23) Stukan, Mikhail, and Wael Abdallah. "Nano-confined adsorbed and free gas in shale reservoirs: A molecular dynamic study." SPE Middle East Oil & Gas Show and Conference. Society of Petroleum Engineers, 2015.

(24) Welch, William RW, and Mohammad Piri. "Molecular Dynamics Simulations of Retrograde Condensation in Narrow Oil-Wet Nanopores." The Journal of Physical Chemistry C119.18 (2015): 10040-10047.

(25) Ambrose, Raymond Joseph, Robert Chad Hartman, Mery Diaz Campos, I. Yucel Akkutlu, and Carl Sondergeld. "New pore-scale considerations for shale gas in place calculations." In *SPE unconventional gas conference*. Society of Petroleum Engineers, 2010.

(26) Javanbakht, Gina, Mohammad Sedghi, William Welch, and Lamia Goual. "Molecular dynamics simulations of CO2/water/quartz interfacial properties: impact of CO2 dissolution in water." *Langmuir* 31, no. 21 (2015): 5812-5819.

(27) Hu, Yinan, Deepak Devegowda, Alberto Striolo, Anh Phan, Tuan A. Ho, Faruk Civan, and Richard Sigal. "The dynamics of hydraulic fracture water confined in nano-pores in shale reservoirs." *Journal of Unconventional Oil and Gas Resources* 9 (2015): 31-39.

(28) Botan, Alexandru, Benjamin Rotenberg, Virginie Marry, Pierre Turq, and Benoît Noetinger. "Carbon dioxide in montmorillonite clay hydrates: thermodynamics, structure, and transport from molecular simulation." *The Journal of Physical Chemistry C* 114, no. 35 (2010): 14962-14969.

(30) Marrink, Siewert J., H. Jelger Risselada, Serge Yefimov, D. Peter Tieleman, and Alex H. De Vries. "The MARTINI force field: coarse grained model for biomolecular simulations." *The journal of physical chemistry B* 111, no. 27 (2007): 7812-7824.

(31) Marrink, Siewert J., Alex H. De Vries, and Alan E. Mark. "Coarse grained model for semiquantitative lipid simulations." *The Journal of Physical Chemistry B* 108.2 (2004): 750-760.

(32) Gražulis, S., Daškevič, A., Merkys, A., Chateigner, D., Lutterotti, L., Quirós, M., Serebryanaya, N. R., Moeck, P., Downs, R. T. & LeBail, A. (2012) "Crystallography Open Database (COD): an open-access collection of crystal structures and platform for world-wide collaboration". *Nucleic Acids Research* **40**, D420-D427

(33) Downs, Robert T., and Michelle Hall-Wallace. "The American Mineralogist crystal structure database." *American Mineralogist* 88, no. 1 (2003): 247-250.

(34) Cygan, Randall T., Jian-Jie Liang, and Andrey G. Kalinichev. "Molecular models of hydroxide, oxyhydroxide, and clay phases and the development of a general force field." *The Journal of Physical Chemistry B* 108.4 (2004): 1255-1266.

(35) van der Spoel, David, Paul J. van Maaren, and Herman JC Berendsen. "A systematic study of water models for molecular simulation: derivation of water models optimized for use with a reaction field." *The Journal of chemical physics* 108.24 (1998): 10220-10230.

(36) Mazyar, Oleg A., Qusai A. Darugar, and Valery N. Khabashesku. "Functions of Nanoparticles and Surfactants in Enhanced Oil Recovery: Molecular Dynamics Studies." *Abu Dhabi International Petroleum Exhibition & Conference*. Society of Petroleum Engineers, (2017).

(37) Wu, Jianyang, Jianying He, Ole Torsater, and Zhiliang Zhang. "Effect of nanoparticles on oil-water flow in a confined nanochannel: a molecular dynamics study." In *SPE international oilfield nanotechnology conference and exhibition*. Society of Petroleum Engineers, 2012.

(38) Bui, Khoa, I. Yucel Akkutlu, Andrei S. Zelenev, William A. Hill, Christian Griman, Trudy C. Boudreaux, and James A. Silas. "Microemulsion effects on oil recovery from kerogen using molecular-dynamics simulation." *SPE Journal* 24, no. 06 (2019): 2541-2554.

(39) He, Shuai, Yang Ning, Tianluo Chen, Honglin Liu, Hongyan Wang, and Guan Qin. "Estimation of transport diffusivity of natural gas in organic matter using molecular dynamics simulation." In *SPE Low Perm Symposium*. Society of Petroleum Engineers, 2016.

(40) Johnson, John E., and Jeffrey A. Speir. "Quasi-equivalent viruses: a paradigm for protein assemblies." *Journal of molecular biology* 269, no. 5 (1997): 665-675.

(41) Shen, V.K., Siderius, D.W., Krekelberg, W.P., and Hatch, H.W., Eds., NIST Standard Reference Simulation Website, NIST Standard Reference Database Number 173, National Institute of Standards and Technology, Gaithersburg MD, 20899, http://doi.org/10.18434/T4M88Q, (retrieved <04/09/2010>).

(42) H. Bekker, H.J.C. Berendsen, E.J. Dijkstra, S. Achterop, R. van Drunen, D. van der Spoel, A. Sijbers, and H. Keegstra *et al.*, "Gromacs: A parallel computer for molecular dynamics simulations"; pp. 252–256 in *Physics computing 92*. Edited by R.A. de Groot and J. Nadrchal. World Scientific, Singapore, 1993.

(43) H.J.C. Berendsen, D. van der Spoel, and R. van Drunen, "GROMACS: A message-passing parallel molecular dynamics implementation," *Comp. Phys. Comm.*, **91** 43–56 (1995).

(44) Jorgensen, William L., David S. Maxwell, and Julian Tirado-Rives. "Development and testing of the OPLS all-atom force field on conformational energetics and properties of organic liquids." *Journal of the American Chemical Society* 118.45 (1996): 11225-11236.

(45) Grubmüller, Helmut, Helmut Heller, Andreas Windemuth, and Klaus Schulten. "Generalized Verlet algorithm for efficient molecular dynamics simulations with long-range interactions." *Molecular Simulation* 6, no. 1-3 (1991): 121-142.

(46) Darden, Tom, Darrin York, and Lee Pedersen. "Particle mesh Ewald: An N· log (N) method for Ewald sums in large systems." *The Journal of chemical physics* 98.12 (1993): 10089-10092.

(47) Humphrey, William, Andrew Dalke, and Klaus Schulten. "VMD: visual molecular dynamics." *Journal of molecular graphics* 14, no. 1 (1996): 33-38.

(48) Murata, Ken-ichiro, and Hajime Tanaka. "Surface-wetting effects on the liquid–liquid transition of a single-component molecular liquid." *Nature communications* 1.1 (2010): 1-9.

(49) Zhang, Kaiyi, Fengshuang Du, and Bahareh Nojabaei. "Effect of Pore Size Heterogeneity on Hydrocarbon Fluid Distribution, Transport, and Primary and Secondary Recovery in Nano-Porous Media." *Energies* 13, no. 7 (2020): 1680.